arXiv:astro-ph/0403626v1   26 Mar 2004

Stellar populations associated with the LMC Papillon Nebula[*]

F. Meynadier[1], M. Heydari-Malayeri[1], L. Deharveng[2], V. Charmandaris[3,1], Th. Le Bertre[1],
M .R. Rosa[4,**], D. Schaerer[5,6], and H. Zinnecker[7]

[1] LERMA, Observatoire de Paris, 61 Avenue de l'Observatoire, F-75014 Paris, France
[2] Observatoire de Marseille, 2 Place Le Verrier, F-13248 Marseille Cedex 4, France
[3] Cornell University, Astronomy Department, 106 Space Sciences Bldg., Ithaca, NY 14853, U.S.A.
[4] Space Telescope European Coordinating Facility, European Southern Observatory, Karl-Schwarzschild-Strasse-2, D-85748 Garching bei München, Germany
[5] Observatoire de Genève, 51, Ch. des Maillettes, CH-1290 Sauverny, Switzerland
[6] Laboratoire d'Astrophysique, UMR 5572, Observatoire Midi-Pyrénées, 14, Avenue E. Belin, F-31400 Toulouse, France
[7] Astrophysikalisches Institut Potsdam, An der Sternwarte 16, D-14482 Potsdam, Germany

Abstract. We study the Large Magellanic Cloud Papillon Nebula (N 159-5), a conspicuous High Excitation Blob (HEB) lying in the star forming complex N 159. Using *JHK* near-infrared photometry obtained at the ESO VLT with the ISAAC camera, we examine the stellar populations associated with the Papillon, tracing their history using stellar evolution models. Two populations are revealed: one composed of young, massive stars with an age ~ 3 Myr, and a second consisting of older lower mass stars of age spreading between 1 and 10 Gyr. We analyze the properties of those populations and discuss their significance in the context of N 159. We also estimate that if the star at the center of the Papillon is single its initial mass is ~ 50 $M_\odot$ and it is affected by an extinction A_V ~ 7 mag.

Key words. Stars: early-type – Interstellar Medium: individual objects: N 159 (LMC) – Galaxies: Magellanic Clouds

1. Introduction

The compact H II regions called High-Excitation Blobs (HEB) constitute a rare class of ionized nebulae in the Magellanic Clouds. They are characterized by high excitation, small size, high density, and large extinction compared to typical Magellanic Cloud H II regions. These objects are tightly linked to the early stages of massive star formation, when the stars begin to hatch from their parental molecular clouds. For this reason their study yields valuable information for a better understanding of the formation of massive stars.

The N 159 complex (Henize 1956) lies south of the famous starburst site 30 Dor and has attracted special attention over the years. Its other designations are MC 77 (McGee et al. 1972), LH 105 (Lucke & Hodge 1970), and DEM 271 (Davies et al. 1976). It shows several signs of ongoing star formation activity, such as infrared sources, cocoon stars, masers, and is also

associated with the most important concentration of molecular gas in the LMC (Jones et al. 1986; Brooks & Whiteoak 1997; Johansson et al. 1998). The molecular emission is in fact due to three distinct giant molecular clouds, known as N159-East, N159-West, and N159-South. Molecular lines tracing high density regions are observed towards N 159-W and N 159-S in CS, CN, HCN, and HCO$^+$ (Heikkilä et al. 1999), while ^{13}CO and upper-level ^{12}CO transitions, and the [C II] emission line were mapped towards the three giant molecular clouds, including N 159-E (Bolatto et al. 2000). The region we are interested in lies near N 159-E.

The Papillon Nebula, also called N 159-5, to which the present study is devoted, is the prototype of the HEB family (Heydari-Malayeri & Testor 1982), which now possesses several members, such as N 160A1, N 160A2, N 83B, N 11A in the LMC and N 88A and N 81 in the SMC. Recent *HST* observations have resolved most of these objects and revealed turbulent media typical of newborn massive star regions marked by strong stellar winds interacting with the ambient ionized gas (Heydari-Malayeri et al. 1999c,a,b, 2001b,a, 2002a,b). These observations also showed a large extinction due to local dust associated with ionized gas. In a number of cases the exciting sources were uncovered as a small cluster of

---

Send offprint requests to: Frédéric Meynadier,
Frederic.Meynadier@obspm.fr

[*] Based on observations obtained at the European Southern Observatory, Paranal, Chile; Program 66.C-0172(A). Table 1 is published only in electronic form.

[**] Affiliated to the Space Telescope Division of the European Space Agency, ESTEC, Noordwijk, Netherlands

Fig. 1. *JHK* color composite image of LMC N 159 (Ks = red, H = green, J = blue) centered on N 159-5, the Papillon nebula. North is up and East is left. See Fig. 2 for star identifications. The field size is $2'.1 \times 2'.2$ ($32\,\mathrm{pc} \times 33\,\mathrm{pc}$).

massive stars.

In particular, the WFPC2 *HST* observations revealed that the featureless blob N 159-5 has in fact the morphology of a *"papillon"*, i.e. it is a butterfly-shaped ionized nebula with the "wings" separated by $\sim 2''.3$ (0.6 pc) (Heydari-Malayeri et al. 1999b, hereafter paper I). Moreover, two subarcsecond features resembling a "smoke ring" and a "globule" were detected in the wings. The images also showed a large number of subarcsecond filaments, arcs, ridges, and fronts carved in the
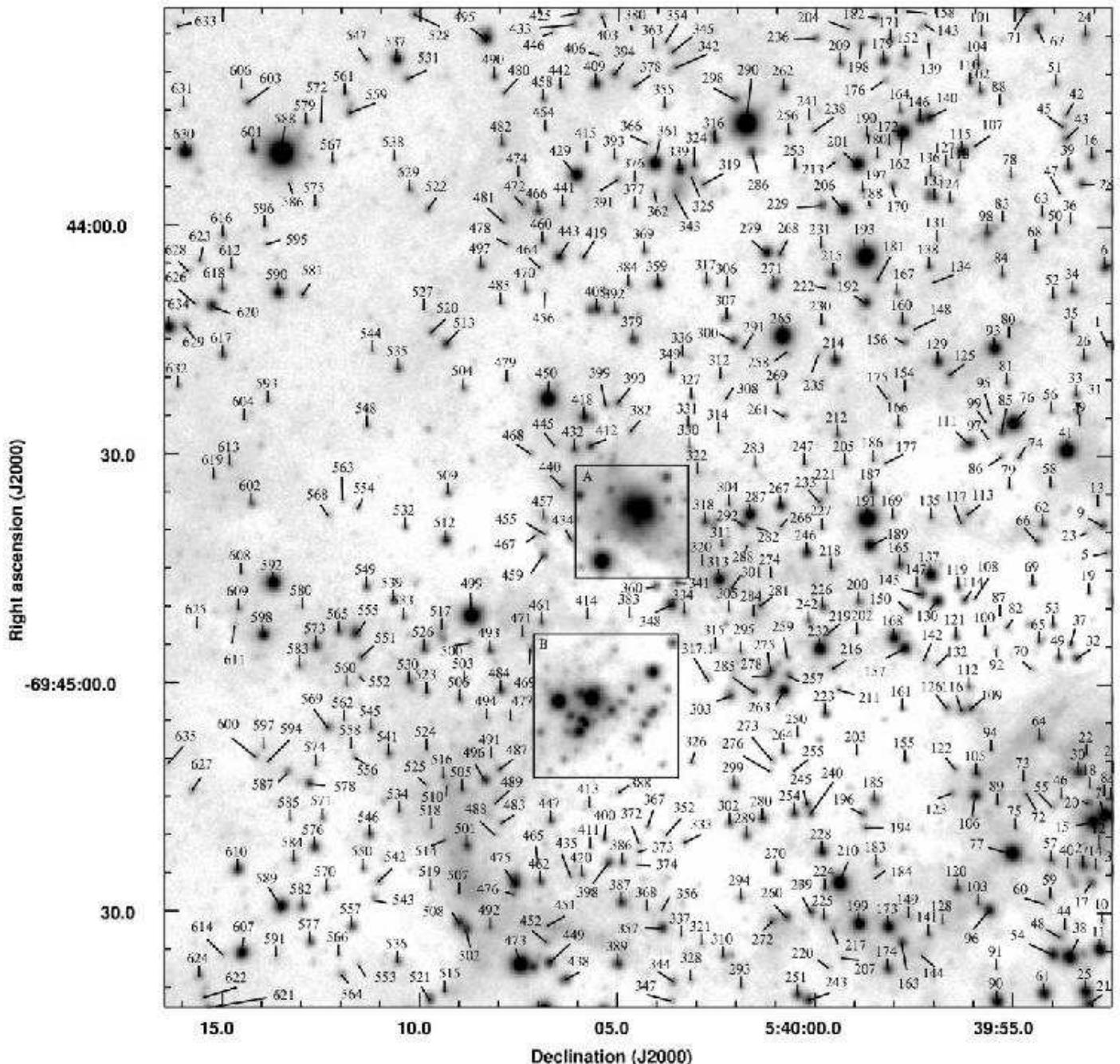
Fig. 2. Finding chart (*H* filter) for the stars in Fig. 1. The numbers refer to Table 1. Regions A (N 159-5) and B are detailed below.
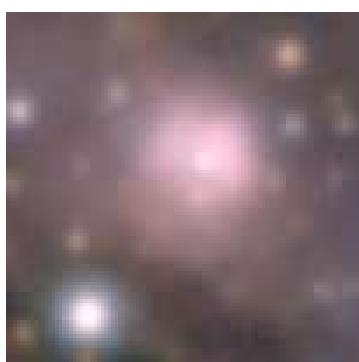

Fig. 3. Composite *JHKs* image (*Ks* = red, *H* = green, *J* = blue) and the corresponding finding chart (*H* band) for region A, the central Papillon (see Paper I).
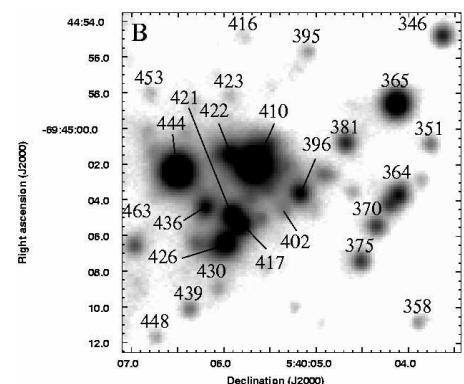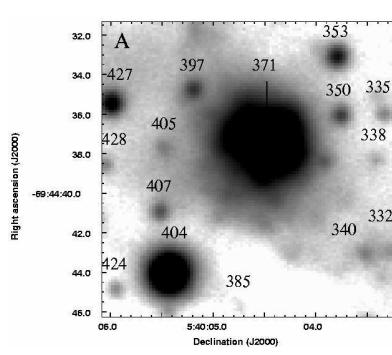

Fig. 4. Finding chart for region B (*H* band).

ionized gas by the stellar winds from massive stars in the N 159 complex. However, no bright stars associated with the core of N 159-5 could be identified in the *HST* images. Could this be due to the extinction by dust large enough to hide the exciting stars? Since an $A_V \geq 6$ mag was needed to bring an O8 star below our *HST* sensitivity limit, we decided to perform high resolution near-IR imaging of the region with the ESO Very Large Telescope in order to address this issue and explore the properties of the stellar population of N 159.

2. Observations and data reduction

The N 159 region was observed in service mode with the ESO Very Large Telescope (VLT). The infrared spectro-imager ISAAC was used at the Nasmyth B focus of UT1 through filters *J* on 7 October and *H* and *Ks* on 1st March 2001. The IR detector (Hawaii Rockwell array) had 1024×1024 pixels of $18.5\,\mu$m each ($0''.148$ on the sky), thus providing a field of $2'.5^2$.

A set of individual, 10-second exposures was obtained in each filter using the dithering method with a random offset of $15''$ at most. The number of exposures were 10, 30, and 36 for the *J*, *H*, and *Ks* bands respectively. The coadded frames have a spatial resolution of $1''.08$ for *J*, $0''.74$ for *H*, and $0''.63$ for *Ks*.

PSF-fitting photometry was carried out in the *J*, *H*, and *Ks* filters using the DAOPHOT II/ALLSTAR procedures (Stetson 1987) under the ESO MIDAS reduction package. It should be noted that these procedures are well adapted to the high-precision photometry of globular clusters (i.e. tight groups of point sources with no background emission), but are not designed for handling regions with very bright and variable background such as N 159. Some alternatives to address those limitations have been investigated by Deharveng et al. (1992), and involve an iterative subtraction of the background as derived from the approximative photometry obtained at each step. In order to improve this method, we developed a software, called DENEB for DE-NEBulized photometry. Our software enables an interactive modification of the intermediate photometry files as well as a real time check of the validity and convergence of those modifications since it displays the resulting residual background.[1]

Finally the frames were calibrated using the mean atmospheric extinction coefficients and the color equations supplied by ESO, and three standard stars for determining the zero points. The average photometric errors reported by DAOPHOT are 0.04, 0.04, and 0.05 mag for the faintest stars in *J*, *H*, and *Ks* respectively. The relative accuracy is better than 0.01 mag for *J*, *H*, and *Ks* brighter than 17 mag.

We compared the resulting magnitudes with those provided by the 2MASS point source catalogue (Cutri et al. 2003a) using a selection of 36 stars which appeared as single in our

---

[1] People interested in the use or development of this tool are invited to contact Frederic.Meynadier@obspm.fr.

frames and were brighter than 15.0 mag in *H*. After correction for filter bandpasses (Carpenter 2001; Cutri et al. 2003b) the mean differences are m(2MASS) − m(ISAAC) = −0.06, −0.08, and −0.02 mag in *J*, *H*, and *Ks* respectively. Taking into account the accuracy of the 2MASS photometry for stars of $H = 15$ mag ($\sim \pm 0.1$ mag r.m.s) and the uncertainties involved in the filter bandpass corrections, we considered these mean differences not to be significant.

Our astrometry and image registration was tied to the positions of the same 2MASS stars since it is known that the r.m.s uncertainty in the positions of the 2MASS catalogue is $< 0''.3$. The astrometry and the photometry of the stars are given in Table 1, which is available in electronic form as online material and also at the Centre de Données astronomiques de Strasbourg (via anonymous ftp to cdsarc.u-strasbg.fr or via http://cdsweb.u-strasbg.fr/Abstract.html).

3. Results

3.1. Morphology

A composite color *JHKs* image of the observed field is shown in Fig. 1, while the corresponding finding chart is presented in Fig. 2. The stars are identified by a number, according to Table 1. Figs. 3 and 4 give details on two densely populated regions, the central Papillon nebula and a small southern cluster.

The field is fairly rich, with 896 stars detected at a 3σ level in the *H* band image (limiting magnitude 20), which has the best S/N ratio. Among them 605 objects are detected at 3σ on all theses frames. Some particularly bright, but highly reddened stars do not appear in all three filters and consequently they were not included in the analysis. Exception was made for a source labeled as #317.1 which is not detected in the *J* band while being relatively bright in *Ks*.

The image is marked by several dark regions and lanes indicating strong absorption. The Papillon nebula is situated near the border of a prominent central absorption lane. The background is dominated by ionized gas emission but is locally obscured by heavy extinction. The southern edge of the field yields a fan-shaped filament already visible on the *HST* frames (Paper I). Our new *JHKs* imagery provides a deeper overview of the stellar content of N 159. We can easily note that the small, bright cluster south to the Papillon (area B of Fig. 2) is much more visible in the near IR than in the optical (Paper I). The two reddest stars of the field are #210 and #317.1. The first one is located in the lower right quadrant of our images almost 1 arcmin from N 159-5, and the second one near the edge of the absorption lane.

We also note the presence of a number of "peculiar" objects having an elongated form and a red color: #343, #517, and #149. The first one seems also to have a tilted shape. The probability that they result from a chance alignment of several faint red stars is very low. Since they are physically too ex-

tended to be considered as circumstellar disks of the LMC, it is more likely that they are simply background galaxies.

3.2. The infrared colors and stellar ages

Fig. 5 presents the Ks versus $H - Ks$ diagram for the measured stars towards N 159, while Fig. 6 displays the corresponding color-color $J - H$ versus $H - Ks$ diagram. All sources brighter than $H = 20$ mag and also detected in J and Ks are taken into account. Star #317.1, which is not detected in J, is assigned an upper limit of 20 in this band. We wish to point several stars in our sample which display rather unique properties. The square in Figs. 5 and 6, identifies star #371, which is the central point-like source of the Papillon. The eight triangles correspond to the brightest components of the small southern cluster marked as region B on Fig. 2.

The color-magnitude and color-color diagrams are interpreted by overplotting isochrones from Lejeune & Schaerer (2001) with Z = 0.008 for a distance modulus of 18.5 mag. As usual with near-IR observations, it is difficult to discriminate low-mass old stars from young massive stars, because the evolutionary tracks are nearly parallel to isochrones, resulting in a very close location on the color-color diagram for those two populations. This degeneracy is lifted if the mass is taken into account: color-magnitude and color-color diagrams should be "coherent", in the sense that populations found to be fitted by a given isochrone in one diagram should be fitted by the same isochrone, within the same mass interval, in the second. Uncertainties in the photometry though, as well as lack of knowledge in the variation of the extinction introduce limitations to the precise determination of the corresponding isochrone.

The diagrams show the presence of two stellar populations. The first one is a young population which appears to be fitted well with a 3 Myr isochrone. Some of the members of this population are weakly affected by extinction while other members have reddened colors. The extinction-free subset is vertically aligned around $H - Ks = 0.00$ in Fig. 5, and the sample affected by extinction has $H - Ks$ colors around 0.20 mag. This young population is made up of massive O type stars, and may also contain a component of reddened B type stars of $\sim 15\,M_\odot$ spread around $H - Ks = 0.2$ mag. Apart from this young population, there is a second population with generally redder colors, which can be fitted with much older isochrones of least 1 to 10 Gyr in age. The bulk of the stars in this population are fainter than $Ks = 17$ mag and have a mass of about $1\,M_\odot$, although the brightest members have evolved into giants. This population is also affected by a varying amount of extinction. The points lying to the right of the 1-10 Gyr isochrones are much more extincted, probably representing the stars situated deeper in the molecular cloud. As was mentioned earlier, it is not clear which precise isochrone should be used, because we expect the extinction to be generally high and locally variable. It is, however, evident that this second population is significantly
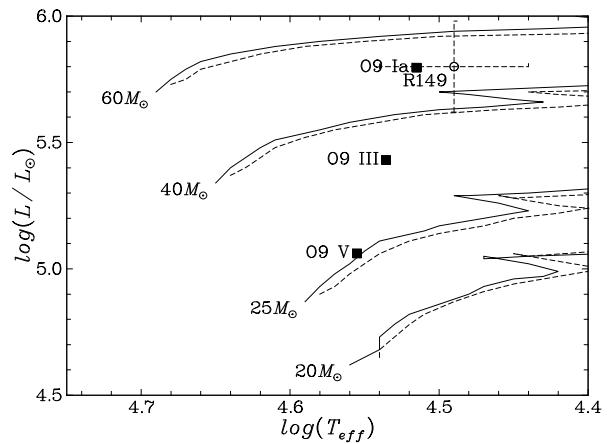
Fig. 7. Evolution tracks for several masses, plotted from the Geneva grid of models (Lejeune & Schaerer 2001). Solid lines: LMC metallicity, Z = 0.008; dashed lines: Galactic metallicity, Z = 0.02. Filled squares represent the positions of O9 type stars of different luminosity class (Vacca et al. 1996)). Open circle shows the position of #193 (R 149), assuming M_V between -6.8 and -6.6, T_{eff} between 27500 and 34300 K, and a bolometric correction between -3.4 and -2.7 (Vacca et al. 1996).

older than the first one, and we can notice the existence of a considerable spread in age among this population. It should also be underlined that for the metallicity of the LMC a star of initial mass $2.15\,M_\odot$ evolves into a giant in less than ~ 1 Gyr.

The color-magnitude diagram can be used to estimate the extinction of the stars. Assuming that the triangles represent young massive stars of age ~ 3 Myr, their shift to the right in Fig. 5 is attributed to reddening by dust. An extinction of $A_V \sim 5$ mag is sufficient to displace the mean position of that stellar population. The star #371, detected towards the Papillon, does not seem to have an IR excess, but is affected by an extinction of $A_V \sim 7$ mag. This is consistent with paper I, which found $A_V \geq 6$ for this central region on the assumption that extinction would have to be large enough to hide an hypothetical O8 exciting star. See Sect. 3.3 for comparison with the CO map.

3.2.1. Isochrone fitting

The apparent magnitude of star #193, better known as R 149 or $Sk-69°257$, is $V = 12.389$ with $B - V = -0.081$, $U - B = -0.962$ mag (Schmidt-Kaler et al. 1999), in agreement with $V = 12.49$ mag (Dufour & Duval 1975), and corresponds to an absolute magnitude of $M_V \sim -6.8$ to -6.6. For an O9 spectral type (Walborn 1977; Conti et al. 1986) this is marginally consistent with luminosity class III, but typical of class I (Vacca et al. 1996). A dwarf classification, as suggested by Conti et al. (1986), seems therefore excluded. The effective temperature of O9 III–I stars is $T_{eff} \sim 34300$–32700 K using Vacca et al.
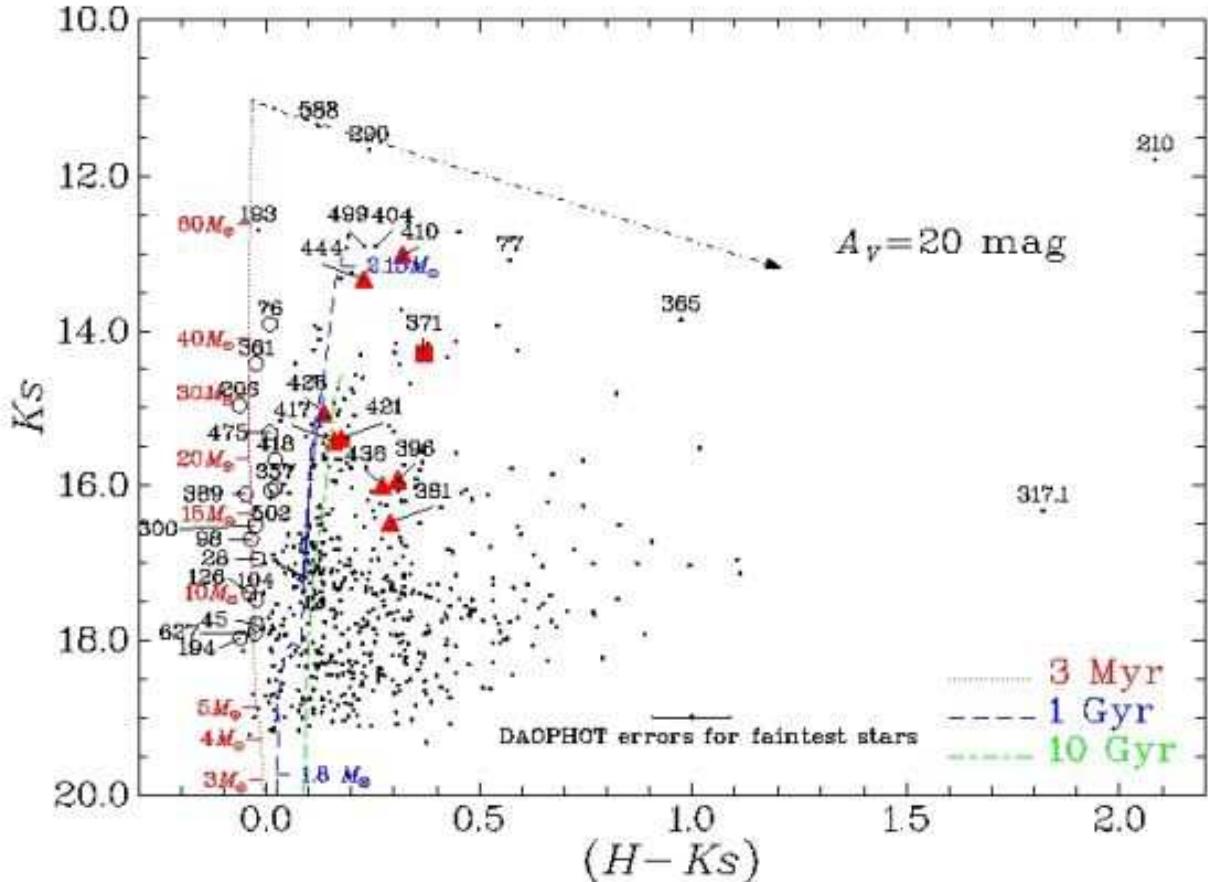
Fig. 5. Color-magnitude, *Ks* versus *H* – *Ks*, diagram for the observed stars towards LMC N 159 detected in all three filters. Three isochrones are shown, 3 Myr (dotted red curve), 1 Gyr (dashed blue), and 10 Gyr (dashed-dotted green), computed for a metallicity of Z = 0.008 (Lejeune & Schaerer 2001) and a distance modulus of 18.5 mag. The upper and lower mass limits are indicated for the 1 Gyr isochrone. The reddening track, plotted as an arrow, extends to $A_V = 20$ mag. The numbers refer to the stellar identifications presented in Fig. 2. Triangles represent a sample of the stars belonging to region B, while the square (numbered #371) refers to the central point-like source of the Papillon. Stars brighter than *Ks* = 18 mag and situated near the 3 Myr isochrone are labelled and shown as empty circles.

(1996)'s calibration or typically between 31.6 and 27500 K for the extreme Ia class based on recent model analysis taking into account non-LTE line blanketing (Martins et al. 2002; Crowther et al. 2002; Herrero et al. 2002; Markova et al. 2004). The bolometric correction, which is essentially independent of line blanketing, is then $BC \sim -3.4$ to -2.7 (Vacca et al. 1996) translating to luminosities $\log L/L_\odot \sim 5.6$–6.0.

Fig. 7 presents the Geneva evolutionary tracks calculated for initial masses 20, 25, 40, and 60 $M_\odot$ and metallicities Z = 0.008 and 0.02 (Lejeune & Schaerer 2001). We reported the position of R 149 on this diagram, using the values calculated in the previous paragraph. It indicates an initial mass of the order of 40 to 60 M$_\odot$, which corresponds to an age of 3 to 5 Myr using the initial masses predicted for stars of various ages and M_V between –6.8 and –6.6 mag (Fig. 8, top). This is consistent with the age range, 1 to 4 Myr, derived from the observed *Ks* magnitude (Fig. 8, bottom).

3.2.2. The brightest and reddest stars

Based on the color-magnitude and color-color diagrams (Figs. 5 & 6), stars #588, #290, #499, #404, #365, #77, and #210 may be high mass main sequence members. These stars can also be very tight multiple systems more or less affected by local dust. In particular, #365 and #210 are very red, probably due to their association with the prominent absorption features in Fig. 1. Furthermore, star #210 presents a near infrared excess typical of some Galactic OB exciting stars, for example star #82 ionizing the H II region Sh2-88B (Deharveng et al. 2000). It is not easy to estimate the extinction and the mass of such a star, more especially since the possible presence of a circumstellar disk alters the colors (Lada & Adams 1992). If single, this star would be one of the most massive stars of the region, having a mass of $\sim 100\, M_\odot$ while affected by an $A_V >$ 20 mag.
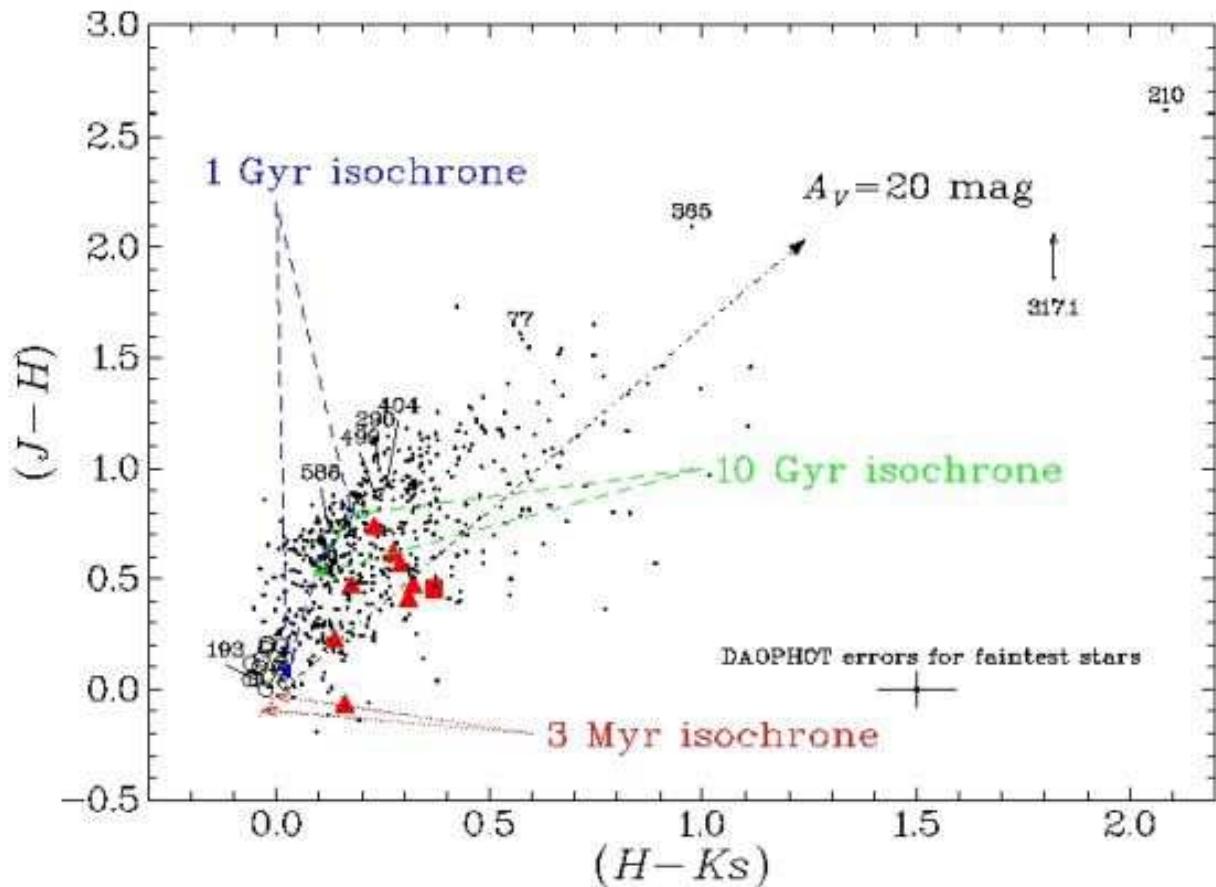
Fig. 6. Color-color, $J − H$ versus $H − Ks$, diagram for the observed LMC N 159 stars. The isochrone reference, symbols, and the reddening track are as in Fig. 5. The arrow attached to star #317.1 is due to the fact that an upper limit of 20 in the J band has been assumed for it.

A number of reasons also suggest that some of these stars may be LMC supergiants. Using a bolometric correction of +2.7 mag in the K band for supergiant stars (van Loon et al. 1999; Le Bertre et al. 2001) and an extinction of $A_K \sim 0.5$ or 1.0 mag, we find that the brightest stars of the sample have an absolute M_K and bolometric M_b magnitudes in the range −8 to −8.5 and −5.7 to −6.2 respectively. These magnitudes are consistent with M type supergiants, carbon stars, or fainter AGB stars in the LMC (van Loon et al. 1999; van Loon 2000). As for #210, which has a redder color of $H − Ks = 2.1$ mag, it can qualify as an LMC AGB candidate. Future spectroscopic observations are needed in order to clarify the nature of these stars.

A third possibility is that at least some of these stars actually belong to our Galaxy and happen to be along the line of sight to the LMC. We can make a rough estimate on their number by establishing the H–R diagram of 2MASS sources found in a field separated by a few degrees from the LMC. It appears that in our field ~ 14 sources brighter than $Ks = 15$ mag might be foreground stars. Those stars cannot be compared to models computed for the LMC distance

modulus. Our observations also indicate that there are 45 stars brighter than $Ks = 15$, so approximately 30 of them should be considered as belonging to the LMC. The above-mentioned bright stars have colors placing them in the low-mass end of any isochrones between 1 to 10 Gyr (Fig. 6) adapted to the LMC, even though they are among the most luminous sources in Fig. 5 where they are located near the high-mass end of the same isochrones. This apparent contradiction can be explained if they are foreground Galactic stars: their location should be compared to "shifted" isochrones in the color-magnitude diagram in order to account for their different distance moduli, while the color-color isochrones would remain unchanged.

3.3. The molecular gas distribution

Johansson et al. (1998) used the ESO SEST (Swedish European Submillimeter Telescope) to map the CO (1–0) emission towards N 159 with a resolution of 40″. We performed a bilinear interpolation between each grid point in order to generate the contours corresponding to the molecular gas associated with the Papillon region. The result, represent-
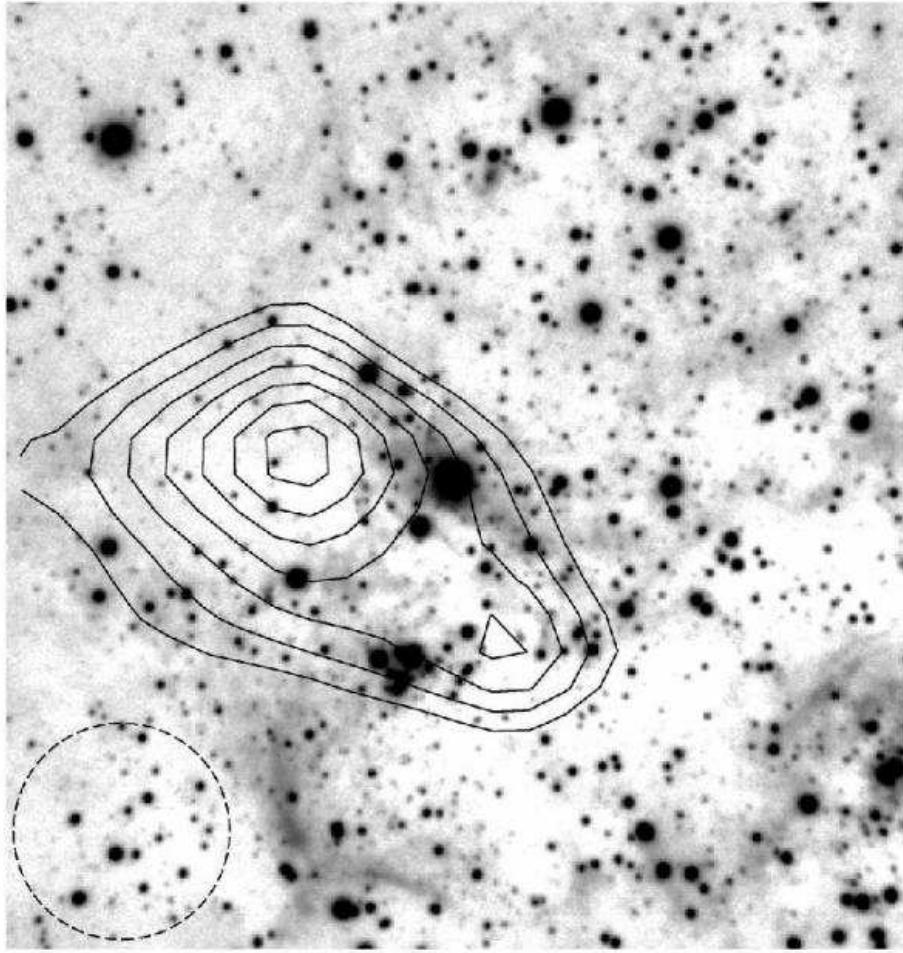
Fig. 9. An H band image of our field with a contour overlay of the ^{12}CO(1–0) intensity of the molecular cloud N159-East from Johansson et al. (1998). The field size and orientation are the same as in Fig. 1, and the SEST $\sim 40''$ ^{12}CO(1–0) beam is marked with a dotted circle.

ing the CO emission peak called N 159-East, is overlayed on the H image and presented in Fig. 9.

The constraints on A_V established in paper I and in the present work are in good agreement with Fig. 9. Since the mapping is relatively scarce, the location of the two peaks cannot be precisely determined but they coincide with the absorption feature bordering the compact H II region. The present picture is in perfect agreement with previous findings that the main CO peak is shifted to the east of the bulk of the giant H II region N 159 mapped in the radio continuum at 843 GHz (Mills & Turtle 1984; Heydari-Malayeri & Testor 1985; Israel et al. 1996). Regions A and B are both adjacent to the molecular peaks, region B being less affected by extinction. It is conceivable that more massive stars be in the process of birth towards the CO emission maxima.

In order to estimate the extinction corresponding to the CO peak the optically thin ^{13}CO transition is needed. Bolatto et al. (2000) observed the N 159-W component in ^{13}CO and derived a column density of 1.1×10^{22} cm^{-2} for the molecular hydrogen H$_2$, corresponding to a column density of atomic hydrogen of 2.2×10^{22} cm^{-2}. It is known that the gas-to-dust ratio $N_H/E(B - V)$ in the LMC is several times larger than the Galactic value (Nandy et al. 1981; Clayton & Martin 1985; Lequeux 1989). Using the conversion relation $N_H/E(B - V) = 2 \times 10^{22}$ atoms cm^{-2} mag^{-1} given by Lequeux (1989) and $R = A_V/E(B - V) = 3.1$, we find a visual extinction of $A_V \sim 3.5$ mag for N 159-W. The extinction for N 159-E should be smaller since we know that N 159-E is less dense than N 159-W (see below). On the other hand, Dickey et al. (1994) carried out 21-cm H I absorption line observations against background continuum sources towards N 159 using the Australia Telescope Compact Array (ATCA) interferometer. Their H I cloud 0539–697 can be identified with the molecular cloud N 159-E, based on velocity similarity (Johansson et al. 1998). The CO cloud has the following characteristics: $V = 238$ km s^{-1}, $\Delta V = 6.0$ km s^{-1}, log(L_{CO}) = 4.28 K km s^{-1} pc^2, whereas those for the H I cloud are: $V = 244$ km s^{-1}, $\Delta V = 1.6$ km s^{-1}, N(H I) = 4.46×10^{22} cm^2. This column density corresponds to a visual extinction of $A_V \sim 7$ mag while that for N 159-W, i.e. N(H I) = 9.62×10^{22} cm^{-2},
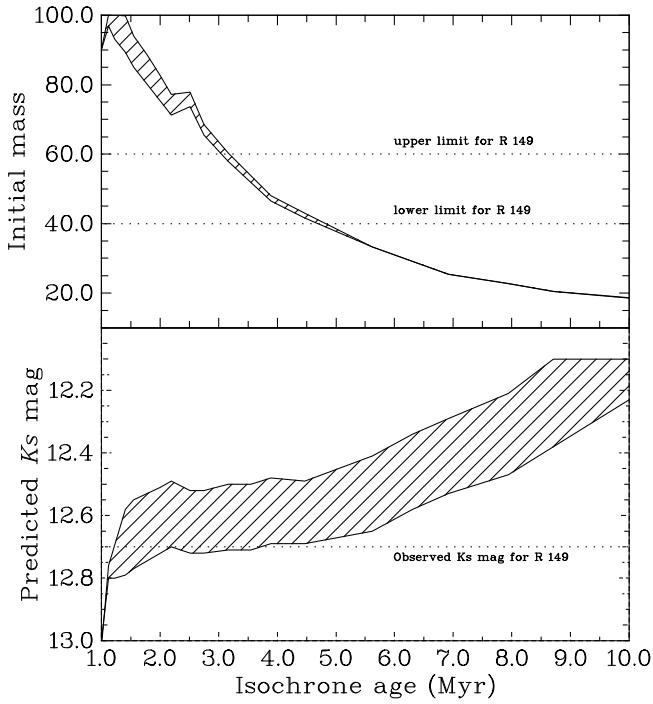
Fig. 8. Expected initial mass (top) and *Ks* magnitude (bottom) for stars with M_V between -6.8 and -6.6 mag as a function of age. The data is taken from the Geneva grid of models for Z = 0.008 (Lejeune & Schaerer 2001). Shaded areas correspond to points with M_V between -6.8 and -6.6. *Top*: The mass range deduced from Fig. 7 is represented by two horizontal dotted line at $M = 60 M_\odot$ and $M = 40 M_\odot$. *Bottom*: The observed *Ks* magnitude is represented by a horizontal dotted line at $Ks = 12.63$ mag.

indicates a larger extinction of $A_V \sim 15$ mag. A reason why H I observations yield stronger extinctions is that the higher spatial resolution of the interferometer picks up denser clumps, in contrast to CO observations which are affected by beam dilution. Moreover, it is quite possible that both techniques do not exactly sample the same zones. Anyhow, the higher values are supported by our *HST* (Paper I) and present ISAAC observations.

4. Discussion

The population of young massive stars, which was discussed earlier (Sect. 3.2), is spatially distributed over the whole field, while a sample of it, represented by triangles in Figs. 5 and 6, is grouped in a cluster, marked as region B. This grouping is expected given the young age of these stars. How can though one explain the separation between this cluster and the other massive stars which even if they have similar ages are at a considerable distances from the cluster, for example $\sim 70''$ (~ 18 pc) for star #193, one of the most distant? One explanation could be that massive star formation may have taken place simultaneously at different parts of the molecular

cloud. At these locations the molecular material has been fully dissociated and ionized, and we do not observe it now. Alternatively, massive star formation has occurred in cluster B, and subsequently a number of the members have been ejected due to the dynamics of the cluster.

It has been shown that once an embedded cluster forms, three mass evacuation mechanisms work over different timescales to disrupt it (Kroupa 2001): *a*) expulsion of embryonic gas (approximately during the first 0–5 Myr), *b*) mass loss from evolving stars (significant after ~ 3 Myr), and *c*) stellar dynamical evaporation and ejection of stars (all times). Binary-binary collisions are required to produce high velocity escapees to occur in low density clusters (Leonard & Duncan 1988, 1990), although simple calculations suggest that such interactions are rather unlikely. Recently Vine & Bonnell (2003) have studied the dynamics of massive stars in young clusters containing gas and stars. They have shown that the location of massive stars outside the core of the cluster does not exclude their formation in the dense cluster core. The massive stars could have originated in the core, but escaped from that region during the gas expulsion phase. Furthermore, the ejection of the OB stars must have happened during an earlier evolutionary stage when the cluster was most probably more compact than today (Portegies Zwart et al. 1999). Assuming that star #193 has been kicked out of cluster B, an escape velocity of ~ 5.5 km s^{-1} has been necessary for it to reach its observed position after a travel time of 3 Myr. This estimate is a lower limit due to projection on the sky of a three-dimensional configuration in space. Higher velocities are quite possible since escapees can leave their birthplace with velocities up to 100 km s^{-1} or even larger (Leonard & Duncan 1990; Kroupa 1995).

We note also that all the candidate massive stars are devoid of proper nebulosity, in contrast to the Papillon. This fact suggests that the Papillon is probably the youngest visible massive star formation event in the whole field. The strength of the molecular hydrogen emission detected towards the Papillon confirms its nature as a very young star formation region (Israel & Koornneef 1988; Kawara et al. 1988). In fact the observed luminosity of the H$_2$ line $v = 1 - 0$ S(1) towards the Papillon is two times larger than that observed at the Orion source (Kawara et al. 1988). The massive star(s) powering the Papillon have not had enough time to disrupt the H II region. Moreover, the presence of nebulosity excludes the possibility for the Papillon of ejection from cluster B. It is therefore conceivable that the Papillon lies somewhat above or below the mean plane of N 159. We believe that the Papillon is situated at the side nearer to us since it is visible in the optical. We estimate that star #371, which lies towards the center of the Papillon, has a mass of $\sim 50 M_\odot$, even though based on our current resolution we cannot exclude the possibility that the star is multiple. Should other massive stars be embedded inside that nebula, much better spatial resolution and deeper exposures are required in order to uncover them. From our previous *HST* observations we estimated an exciting star of type at least O8 V, $\sim 30 M_\odot$ (Vacca et al. 1996), for the Papillon using the Hβ flux measurement and assuming that

the H II region is ionization bounded (Paper I). The difference between the two mass estimates is due to the fact the H II region is density-bounded at least towards us and that the flux correction for extinction is not straightforward. The latter point is probably the reason why the radio continuum observations, which are less affected by extinction, yield a higher Lyman continuum flux. In an earlier work (Heydari-Malayeri & Testor 1985), we used the radio continuum observations at 843 MHz, obtained with a beam of $43'' \times 46''$, to derive a flux density of 55 mJy for N 159-5, after correcting for contamination by the surrounding field. A resulting ultraviolet flux of $\sim 1.2 \times 10^{49}$ photons indicates an O7 V type star of $\sim 38\, M_\odot$ (Vacca et al. 1996). Given the uncertainties involved, the stellar mass estimates based on the H I emission from the nebula agree well with the $\sim 50\, M_\odot$ derived from photometry using evolutionary models.

An age of ~ 3 Myr was derived for the massive star population using the evolutionary models and supplementary data on one of the members. We wish to note though that this age estimate may not be very accurate due to the degeneracy of the near IR colors of massive stars. In fact any isochrone between 1 and 10 Myrs would be consistent with our data. We favored the 3 Myr isochrone in order to meet the requirements of star Sk$-69°257$.

One can also estimate the number of stars which power the H II region N 159 on the basis of radio continuum observations. Clarke et al. (1976) measured a radio continuum flux density of 6.5 Jy at 408 MHz using the Molonglo telescope whose beam had a width of $2'.6 \times 2'.9$. The beamwidth is comparable with the size of our ISAAC field, and the target coordinates match the position of the Papillon, while the reported pointing accuracy is $18'' \times 5''$. The derived Lyman continuum flux of 1.36×10^{51} photons s^{-1} corresponds to some 40 massive stars of type O5 V with an initial mass of $\sim 50\, M_\odot$ (Vacca et al. 1996). Taking a Salpeter-like initial mass function with slope $x = -1.5$, we can predict the presence of some 360 stars of mass about $10\, M_\odot$ and 3240 stars of $\sim 2\, M_\odot$. Where are these 40 O5 V stars? It is quite possible that they are among the stars we imaged but due to the degeneracies in the colors mentioned earlier they can only be clearly identified if spectroscopic observations were available. Moreover, some of them may be embedded in the molecular cloud and some situated outside our ISAAC field.

The color-mag diagram (Fig. 5) also shows the presence of intermediate mass stars of ~ 4–$10\, M_\odot$ on the main sequence formed together with high mass stars ~ 3 Myr ago. This is in agreement with more detailed results on the Orion Nebular Cluster (ONC) based on a large body of data (~ 3500 stars identified within ~ 2.5 pc of the Trapezium, among which at least ~ 1600 with photometric and spectroscopic data in the visible) (Hillenbrand 1997). According to these studies, low-, intermediate-, and high-mass stars have formed together in the ONC a few Myr ago (Palla & Stahler 1999). However, this may not be a universal trend since Herbst & Miller (1982)'s study of NGC 3293 led them to the conclusion that in a cluster low- and intermediate-mass stars form first, with the process continuing gradually until the high-mass stars appear. This result is in agreement with more recent findings on star formation in LMC clusters and associations. For instance, in the case of the R 136 cluster, situated in the LMC 30 Dor, Massey & Hunter (1998) arrived to the conclusion that intermediate-mass stars began forming some 6 Myr ago and continued up to the time when the high-mass stars formed, 1–2 Myr ago.

An interesting question is whether the young (~ 3 Myr) and old (~ 1–10 Gy) stellar populations have formed in the same region of space. Although presently we do not have the necessary data to address this issue and cannot reach a firm conclusion, it is quite possible that both populations be spatially unrelated. The LMC is known to have a considerable depth, the old population can have formed in a different depth during much earlier star formation activities. In order to get some insight about this question, we used the 2MASS data to probe a bare stellar field devoid of any particular nebular emission lying near the N 159 complex (radius $1'.22$, centered on $\alpha = 05h\,39m\,00s$, $\delta = -69°\,47'30''$). The corresponding HR diagram shows the absence of a young, unreddened population, but the presence of an old population resembling the one found towards N 159. Although this population is relatively smaller in number with respect to that of N 159, since 2MASS is not as deep as our photometry, the presence of the old population is certain. The old population seems therefore to be a common background stellar component towards this part of the LMC.

The presence of low-mass pre-main sequence LMC stars in the above diagrams seems unlikely, even if those objects are characterized by large near IR colors, $H - K \sim 1.5$ mag (Lada & Adams 1992; Chabrier et al. 2000). A pre-main sequence star of $\sim 1\, M_\odot$ has a luminosity of $\log(L/L_\odot) \sim 1$ on its birthline, corresponding to an observed visual magnitude of ~ 21, which is below our detection limit. An intermediate mass pre-main sequence star of $5\, M_\odot$ has an effective temperature of $\sim 11,000$ K and $\log(L/L_\odot) \sim 3$, corresponding to a reddened 16 magnitude star, occupying loci around $J - H \sim 0.5$ and $H - K = 0.5$ mag (Lada & Adams 1992). There is a few number of sources with such colors in Fig. 6, given the color uncertainties at those magnitudes. Therefore, we cannot exclude the possibility that some of those points represent intermediate mass PMS stars. As for more massive objects, the concept of pre-main sequence is not applicable to stars above $\sim 6\, M_\odot$ since the birthline and the ZAMS unify at those mass levels (Palla & Stahler 1993).

Comparison between LMC N 159 and SMC N 81 points out dramatic differences between the environments of these two HEBs. The present work shows the Papillon as part of a rich complex containing a large molecular cloud and a cluster of young, massive stars, whereas our previous study of SMC N 81, based on ISAAC near IR observations (Heydari-Malayeri et al. 2003), revealed a solitary star formation event. Moreover, since the two compact H II regions have several comparable characteristics, if we assume that they

have gone through a similar formation process, then the HEB formation can take place in both very dense as well as rather sparse environments.

References

Bolatto, A. D., Jackson, J. M., Israel, F. P., Zhang, X., & Kim, S. 2000, ApJ, 545, 234

Brooks, K. J. & Whiteoak, J. B. 1997, MNRAS, 291, 395

Carpenter, J. M. 2001, AJ, 121, 2851

Chabrier, G., Baraffe, I., Allard, F., & Hauschildt, P. 2000, ApJ, 542, 464

Clarke, J. N., Little, A. G., & Mills, B. Y. 1976, Australian Journal of Physics Astrophysical Supplement, 40, 1

Clayton, G. C. & Martin, P. G. 1985, ApJ, 288, 558

Conti, P. S., Garmany, C. D., & Massey, P. 1986, AJ, 92, 48

Crowther, P. A., Hillier, D. J., Evans, C. J., et al. 2002, ApJ, 579, 774

Cutri, R. M., Skrutskie, M. F., van Dyk, S., et al. 2003a, VizieR Online Data Catalog, 2246, 0

Cutri, R. M., Skrutskie, M. F., van Dyk, S., et al. 2003b, Explanatory Supplement to the 2MASS All Sky Data Release (Pasadena: Caltech), www.ipac.caltech.edu/2mass/releases/allsky/doc/

Davies, R., Eliott, K., & Meaburn, J. 1976, Mem. R. Astron. Soc., 81, 89

Deharveng, L., Caplan, J., & Lombard, J. 1992, A&AS, 94, 359

Deharveng, L., Nadeau, D., Zavagno, A., & Caplan, J. 2000, A&A, 360, 1107

Dickey, J. M., Mebold, U., Marx, M., et al. 1994, A&A, 289, 357

Dufour, R. J. & Duval, J. E. 1975, PASP, 87, 769

Heikkilä, A., Johansson, L. E. B., & Olofsson, H. 1999, A&A, 344, 817

Henize, K. G. 1956, ApJS, 2, 315

Herbst, W. & Miller, D. P. 1982, AJ, 87, 1478

Herrero, A., Puls, J., & Najarro, F. 2002, A&A, 396, 949

Heydari-Malayeri, M., Charmandaris, V., Deharveng, L., et al. 2002a, A&A, 381, 941

Heydari-Malayeri, M., Charmandaris, V., Deharveng, L., et al. 2001a, A&A, 372, 527

Heydari-Malayeri, M., Charmandaris, V., Deharveng, L., et al. 2001b, A&A, 372, 495

Heydari-Malayeri, M., Charmandaris, V., Deharveng, L., Rosa, M. R., & Zinnecker, H. 1999a, A&A, 347, 841

Heydari-Malayeri, M., Meynadier, F., Charmandaris, V., et al. 2003, A&A, 411, 427

Heydari-Malayeri, M., Rosa, M. R., Charmandaris, V., Deharveng, L., & Zinnecker, H. 1999b, A&A, 352, 665, **paper I**

Heydari-Malayeri, M., Rosa, M. R., Schaerer, D., Martins, F., & Charmandaris, V. 2002b, A&A, 381, 951

Heydari-Malayeri, M., Rosa, M. R., Zinnecker, H., Deharveng, L., & Charmandaris, V. 1999c, A&A, 344, 848

Heydari-Malayeri, M. & Testor, G. 1982, A&A, 111, L11

Heydari-Malayeri, M. & Testor, G. 1985, A&A, 144, 98

Hillenbrand, L. A. 1997, AJ, 113, 1733

Israel, F. P. & Koornneef, J. 1988, A&A, 190, 21

Israel, F. P., Maloney, P. R., Geis, N., et al. 1996, ApJ, 465, 738

Johansson, L. E. B., Greve, A., Booth, R. S., et al. 1998, A&A, 331, 857

Jones, T. J., Hyland, A. R., Straw, S., et al. 1986, MNRAS, 219, 603

Joye, W. A. & Mandel, E. 2003, in ASP Conf. Ser. 295: Astronomical Data Analysis Software and Systems XII, 489

Kawara, K., Taniguchi, Y., & Nishida, M. 1988, PASP, 100, 458

Kroupa, P. 1995, MNRAS, 277, 1522

Kroupa, P. 2001, in ASP Conf. Ser. 243: From Darkness to Light: Origin and Evolution of Young Stellar Clusters, 387

Lada, C. J. & Adams, F. C. 1992, ApJ, 393, 278

Le Bertre, T., Matsuura, M., Winters, J. M., et al. 2001, A&A, 376, 997

Lejeune, T. & Schaerer, D. 2001, A&A, 366, 538

Leonard, P. J. T. & Duncan, M. J. 1988, AJ, 96, 222

Leonard, P. J. T. & Duncan, M. J. 1990, AJ, 99, 608

Lequeux, J. 1989, in Recent Developments of Magellanic Cloud Research. A European Colloquium, held in Paris, France, May 9-11, 1989. Editors, K.S. de Boer, F. Spite, G. Stasinska; Publisher, Observatoire de Paris, Section Astrophysique de Meudon, Meudon, France, 1989., 119

Lucke, P. B. & Hodge, P. W. 1970, AJ, 75, 171

Markova, N., Puls, J., Repolust, T., & Markov, H. 2004, Accepted by A&A

Martins, F., Schaerer, D., & Hillier, D. J. 2002, A&A, 382, 999

Massey, P. & Hunter, D. A. 1998, ApJ, 493, 180

McGee, R. X., Brooks, J. W., & Batchelor, R. A. 1972, Australian Journal of Physics, 25, 581

Mills, B. Y. & Turtle, A. J. 1984, in IAU Symp. 108: Structure and Evolution of the Magellanic Clouds, 283–290

Nandy, K., Morgan, D. H., Willis, A. J., Wilson, R., & Gondhalekar, P. M. 1981, MNRAS, 196, 955

Palla, F. & Stahler, S. W. 1993, ApJ, 418, 414

Palla, F. & Stahler, S. W. 1999, ApJ, 525, 772

Portegies Zwart, S. F., Makino, J., McMillan, S. L. W., & Hut, P. 1999, A&A, 348, 117

Schmidt-Kaler, T., Gochermann, J., Oestreicher, M. O., et al. 1999, MNRAS, 306, 279

Stetson, P. B. 1987, PASP, 99, 191

Vacca, W. D., Garmany, C. D., & Shull, J. M. 1996, ApJ, 460, 914

van Loon, J. T. 2000, A&A, 354, 125

van Loon, J. T., Groenewegen, M. A. T., de Koter, A., et al. 1999, A&A, 351, 559

Vine, S. G. & Bonnell, I. A. 2003, MNRAS, 342, 314

Walborn, N. R. 1977, ApJ, 215, 53

Online Material

Table 1. Astrometry and photometry of sources, with DAOPHOT errors

ID	RA (J 2000.0)	DEC (J 2000.0)	J (mag)	H (mag)	Ks (mag)	σJ	σH	σKs	notes
3	05:39:52.52	-69:45:24.9	18.32	18.31	18.18	0.019	0.031	0.031	
4	05:39:52.55	-69:45:14.9	17.54	17.26	17.17	0.009	0.018	0.012	
5	05:39:52.66	-69:44:42.7	18.50	17.83	17.56	0.014	0.011	0.011	
6	05:39:52.71	-69:44:05.3	16.04	16.03	15.99	0.005	0.003	0.004	
7	05:39:52.71	-69:45:17.2	14.22	14.04	13.93	0.004	0.005	0.004	
8	05:39:52.71	-69:45:14.6	19.03	18.65	18.38	0.038	0.040	0.041	
9	05:39:52.77	-69:44:39.1	17.45	16.53	16.21	0.007	0.006	0.006	
10	05:39:52.77	-69:45:31.2	18.90	18.31	18.14	0.017	0.020	0.021	
11	05:39:52.84	-69:45:34.8	15.49	14.71	14.59	0.005	0.008	0.011	
13	05:39:52.89	-69:44:36.5	19.46	18.87	18.54	0.028	0.027	0.022	
14	05:39:52.92	-69:45:24.2	19.04	17.95	17.67	0.023	0.012	0.015	
15	05:39:53.01	-69:45:18.0	14.65	14.36	14.25	0.006	0.005	0.006	
16	05:39:53.05	-69:43:50.9	17.68	17.07	17.00	0.008	0.006	0.008	
17	05:39:53.05	-69:45:26.0	17.31	16.83	16.79	0.007	0.008	0.011	
18	05:39:53.08	-69:45:13.6	19.57	19.02	18.61	0.047	0.063	0.043	
19	05:39:53.11	-69:44:48.0	18.80	18.36	18.34	0.013	0.021	0.023	
20	05:39:53.12	-69:45:15.6	17.36	17.00	17.00	0.014	0.012	0.012	
21	05:39:53.12	-69:45:41.9	16.74	16.03	15.92	0.014	0.007	0.011	
22	05:39:53.16	-69:45:09.3	18.80	18.55	18.23	0.024	0.025	0.026	
23	05:39:53.18	-69:44:40.0	19.65	18.87	18.46	0.042	0.028	0.026	
24	05:39:53.21	-69:43:34.8	17.57	17.28	17.16	0.012	0.010	0.012	
25	05:39:53.20	-69:45:40.3	15.76	15.00	14.80	0.006	0.005	0.008	
26	05:39:53.23	-69:44:17.3	18.14	17.22	16.95	0.008	0.006	0.008	
27	05:39:53.26	-69:45:23.8	16.85	16.16	16.10	0.006	0.005	0.007	
28	05:39:53.31	-69:43:54.4	17.13	16.93	16.95	0.007	0.006	0.008	
29	05:39:53.35	-69:44:25.9	19.31	18.84	18.76	0.021	0.029	0.032	
30	05:39:53.37	-69:45:11.6	16.40	15.86	15.75	0.012	0.025	0.039	
31	05:39:53.39	-69:44:24.5	18.04	17.93	17.93	0.009	0.011	0.016	
32	05:39:53.43	-69:44:56.6	17.53	16.85	16.79	0.010	0.007	0.008	
33	05:39:53.44	-69:44:22.1	17.82	17.38	17.31	0.008	0.007	0.009	
34	05:39:53.52	-69:44:08.5	17.10	16.92	16.90	0.006	0.005	0.006	
35	05:39:53.54	-69:44:13.7	18.45	17.55	17.32	0.015	0.008	0.009	
36	05:39:53.58	-69:43:59.5	19.50	18.74	18.73	0.027	0.024	0.031	
37	05:39:53.57	-69:44:54.7	18.11	17.42	17.24	0.011	0.008	0.011	
38	05:39:53.60	-69:45:35.8	14.55	14.24	14.11	0.003	0.004	0.006	
39	05:39:53.64	-69:43:52.3	17.30	16.69	16.63	0.008	0.004	0.006	
40	05:39:53.65	-69:45:24.1	19.39	18.73	18.45	0.048	0.027	0.028	
41	05:39:53.67	-69:44:29.3	14.39	13.50	13.33	0.004	0.001	0.003	
42	05:39:53.69	-69:43:45.3	19.05	18.22	17.58	0.016	0.016	0.012	
43	05:39:53.69	-69:43:48.4	18.12	17.23	17.04	0.011	0.008	0.013	
44	05:39:53.71	-69:45:32.1	19.30	18.50	18.29	0.034	0.025	0.028	
45	05:39:53.77	-69:43:46.8	17.98	17.77	17.79	0.011	0.010	0.013	
46	05:39:53.80	-69:45:14.9	19.37	18.65	18.38	0.025	0.022	0.026	
47	05:39:53.84	-69:43:55.7	19.86	19.23	19.04	0.031	0.030	0.043	
48	05:39:53.84	-69:45:33.1	18.06	17.62	17.50	0.032	0.012	0.011	
49	05:39:53.87	-69:44:56.6	17.73	17.09	17.05	0.015	0.007	0.010	
50	05:39:53.94	-69:44:00.9	19.44	18.49	18.19	0.022	0.018	0.018	
51	05:39:53.96	-69:43:41.4	18.33	17.97	17.94	0.011	0.011	0.014	
52	05:39:54.01	-69:44:09.3	18.31	17.77	17.73	0.012	0.010	0.011	
53	05:39:54.01	-69:44:52.3	18.17	17.54	17.25	0.011	0.010	0.010	
54	05:39:54.02	-69:45:35.4	16.21	15.46	15.36	0.011	0.004	0.007	
55	05:39:54.03	-69:45:16.0	19.88	18.15	17.72	0.036	0.021	0.021	
56	05:39:54.06	-69:44:24.3	18.79	18.30	18.27	0.015	0.017	0.018	

Table 1. continued...

ID	RA (J 2000.0)	DEC (J 2000.0)	J (mag)	H (mag)	Ks (mag)	σJ	σH	σKs	notes
57	05:39:54.06	-69:45:23.2	17.64	17.16	17.04	0.009	0.008	0.009	
58	05:39:54.08	-69:44:34.0	18.99	18.47	18.28	0.021	0.018	0.021	
59	05:39:54.08	-69:45:28.0	18.41	17.98	18.01	0.014	0.013	0.021	
60	05:39:54.23	-69:45:28.8	18.88	18.63	18.46	0.026	0.024	0.028	
61	05:39:54.25	-69:45:40.6	15.74	15.20	15.17	0.005	0.006	0.007	
62	05:39:54.27	-69:44:39.1	17.42	16.84	16.75	0.006	0.004	0.005	
63	05:39:54.30	-69:43:58.6	18.74	18.44	18.35	0.015	0.016	0.016	
64	05:39:54.35	-69:45:07.2	17.63	17.16	17.10	0.009	0.009	0.013	
65	05:39:54.36	-69:44:54.5	18.73	17.66	17.40	0.016	0.015	0.009	
66	05:39:54.41	-69:44:41.3	17.77	17.18	17.12	0.009	0.007	0.008	
67	05:39:54.43	-69:43:34.0	17.03	16.43	16.19	0.011	0.004	0.006	
68	05:39:54.46	-69:44:03.0	18.48	17.62	17.38	0.013	0.009	0.009	
69	05:39:54.54	-69:44:46.9	18.52	17.58	17.33	0.012	0.008	0.008	
70	05:39:54.56	-69:44:58.0	19.54	18.70	18.50	0.027	0.026	0.021	
71	05:39:54.72	-69:43:31.1	15.75	14.59	14.14	0.033	0.019	0.016	
72	05:39:54.73	-69:45:14.4	19.28	18.09	17.61	0.028	0.016	0.016	
73	05:39:54.76	-69:45:12.7	18.91	18.51	18.20	0.021	0.019	0.027	
74	05:39:54.89	-69:44:30.3	18.75	18.01	17.77	0.014	0.015	0.014	
75	05:39:54.96	-69:45:19.0	19.50	18.49	18.07	0.032	0.023	0.017	
76	05:39:55.02	-69:44:25.8	14.04	13.92	13.91	0.003	0.001	0.003	
77	05:39:55.05	-69:45:22.2	15.27	13.66	13.09	0.005	0.002	0.004	
78	05:39:55.09	-69:43:53.5	19.44	18.35	18.03	0.025	0.015	0.013	
79	05:39:55.12	-69:44:34.2	19.06	18.62	18.44	0.016	0.021	0.020	
80	05:39:55.13	-69:44:14.5	19.28	18.91	18.83	0.024	0.025	0.029	
82	05:39:55.19	-69:44:52.6	19.06	18.04	17.70	0.018	0.012	0.016	
83	05:39:55.29	-69:43:59.3	19.27	19.34	19.12	0.031	0.048	0.041	
84	05:39:55.31	-69:44:06.4	18.22	17.55	17.53	0.011	0.010	0.010	
85	05:39:55.32	-69:44:27.0	17.89	16.77	16.54	0.012	0.006	0.007	
86	05:39:55.33	-69:44:30.2	18.29	18.13	18.12	0.010	0.013	0.015	
87	05:39:55.36	-69:44:51.0	19.79	19.24	18.93	0.029	0.041	0.032	
88	05:39:55.37	-69:43:44.0	19.47	18.63	18.42	0.027	0.019	0.026	
89	05:39:55.41	-69:45:15.7	19.27	18.10	17.61	0.027	0.017	0.018	
91	05:39:55.44	-69:45:37.4	19.83	18.97	19.00	0.036	0.038	0.046	
92	05:39:55.46	-69:44:55.3	19.71	18.62	18.36	0.029	0.021	0.022	
93	05:39:55.51	-69:44:16.0	15.62	14.58	14.28	0.004	0.002	0.002	
94	05:39:55.57	-69:45:08.7	19.03	18.42	18.00	0.023	0.015	0.019	
95	05:39:55.58	-69:44:24.5	19.81	19.16	19.14	0.051	0.029	0.043	
96	05:39:55.63	-69:45:29.7	16.25	15.52	15.23	0.005	0.003	0.005	
97	05:39:55.65	-69:44:27.8	19.65	19.09	19.00	0.031	0.032	0.032	
98	05:39:55.69	-69:44:00.9	16.80	16.67	16.70	0.007	0.009	0.009	
99	05:39:55.69	-69:44:25.7	19.34	19.21	19.05	0.031	0.034	0.035	
100	05:39:55.72	-69:44:53.6	18.99	18.06	17.86	0.019	0.011	0.015	
101	05:39:55.83	-69:43:34.9	18.78	17.93	17.62	0.020	0.012	0.011	
102	05:39:55.86	-69:43:42.3	18.02	17.26	17.13	0.006	0.007	0.008	
103	05:39:55.91	-69:45:28.9	18.48	17.67	17.49	0.019	0.011	0.015	
104	05:39:55.92	-69:43:38.7	17.64	17.46	17.48	0.008	0.007	0.012	
105	05:39:55.95	-69:45:11.8	17.86	16.53	15.86	0.010	0.004	0.004	
106	05:39:55.97	-69:45:14.6	16.08	15.60	15.40	0.005	0.004	0.005	
107	05:39:56.01	-69:43:49.4	18.70	18.54	18.52	0.015	0.020	0.024	
108	05:39:56.00	-69:44:48.8	19.52	18.87	18.74	0.030	0.022	0.023	
109	05:39:56.11	-69:45:03.2	17.18	16.89	16.85	0.007	0.005	0.009	
110	05:39:56.12	-69:43:41.1	18.02	17.27	17.14	0.009	0.007	0.008	
111	05:39:56.13	-69:44:28.5	16.88	16.12	15.95	0.010	0.015	0.015	
112	05:39:56.14	-69:45:00.4	18.74	17.69	17.37	0.019	0.009	0.010	
113	05:39:56.17	-69:44:37.7	18.41	17.66	17.36	0.013	0.008	0.010	

Table 1. continued...

ID	RA (J 2000.0)	DEC (J 2000.0)	J (mag)	H (mag)	Ks (mag)	σJ	σH	σKs	notes
114	05:39:56.26	-69:44:48.9	17.83	17.15	16.95	0.009	0.009	0.010	
115	05:39:56.32	-69:43:50.2	16.38	15.59	15.45	0.005	0.003	0.003	
116	05:39:56.32	-69:45:03.4	17.55	17.23	17.17	0.008	0.007	0.009	
117	05:39:56.34	-69:44:38.8	18.68	17.74	17.41	0.018	0.009	0.009	
118	05:39:56.37	-69:43:52.7	18.70	18.21	18.14	0.018	0.021	0.019	
119	05:39:56.41	-69:44:47.3	18.07	17.21	16.96	0.007	0.008	0.009	
120	05:39:56.43	-69:45:26.9	17.10	16.37	16.02	0.007	0.004	0.005	
121	05:39:56.46	-69:44:53.8	18.02	17.27	17.10	0.009	0.008	0.008	
122	05:39:56.48	-69:45:11.2	19.45	18.19	17.81	0.029	0.017	0.017	
123	05:39:56.57	-69:45:14.3	18.57	17.89	17.79	0.016	0.013	0.017	
124	05:39:56.62	-69:43:56.7	18.28	17.61	17.51	0.013	0.009	0.012	
125	05:39:56.64	-69:44:19.4	18.21	17.46	17.22	0.011	0.007	0.010	
126	05:39:56.70	-69:45:03.1	17.45	17.35	17.39	0.009	0.009	0.013	
127	05:39:56.73	-69:43:52.0	18.45	18.09	18.14	0.014	0.013	0.022	
128	05:39:56.80	-69:45:31.5	19.00	18.46	18.14	0.022	0.024	0.028	
129	05:39:56.93	-69:44:17.7	16.76	15.88	15.64	0.007	0.003	0.002	
130	05:39:56.95	-69:44:49.1	16.21	15.43	15.23	0.004	0.002	0.004	
131	05:39:56.95	-69:44:01.8	19.42	19.17	19.16	0.026	0.029	0.038	
132	05:39:56.95	-69:44:57.5	19.20	18.24	17.93	0.017	0.016	0.017	
133	05:39:57.01	-69:43:56.3	16.98	16.98	16.96	0.017	0.012	0.012	
134	05:39:57.07	-69:44:07.4	19.95	19.51	19.08	0.044	0.042	0.041	
135	05:39:57.10	-69:44:38.3	18.56	17.98	17.71	0.015	0.012	0.011	
136	05:39:57.11	-69:43:53.3	17.96	17.87	17.86	0.008	0.010	0.013	
137	05:39:57.12	-69:44:45.6	15.79	14.75	14.44	0.005	0.002	0.002	
138	05:39:57.15	-69:44:05.4	18.23	17.32	17.02	0.009	0.008	0.008	
139	05:39:57.16	-69:43:35.9	18.63	18.58	18.47	0.019	0.018	0.022	
140	05:39:57.16	-69:43:45.7	16.57	15.85	15.67	0.006	0.003	0.004	
141	05:39:57.16	-69:45:32.9	18.17	17.59	17.46	0.012	0.009	0.010	
142	05:39:57.25	-69:44:56.9	19.35	18.70	18.47	0.022	0.022	0.031	
143	05:39:57.26	-69:43:33.5	18.05	18.24	18.14	0.025	0.019	0.020	
144	05:39:57.33	-69:45:35.6	19.24	18.72	18.71	0.024	0.025	0.037	
145	05:39:57.34	-69:44:48.2	17.22	16.32	16.07	0.005	0.004	0.005	
146	05:39:57.38	-69:43:46.0	16.85	15.97	15.77	0.008	0.004	0.004	
148	05:39:57.53	-69:44:13.4	19.17	18.99	18.85	0.026	0.036	0.037	
149	05:39:57.66	-69:45:30.6	19.72	18.26	17.14	0.036	0.032	0.052	
150	05:39:57.68	-69:44:50.3	17.57	17.29	17.20	0.007	0.006	0.007	
152	05:39:57.74	-69:43:37.6	17.64	16.92	16.84	0.008	0.006	0.007	
154	05:39:57.75	-69:44:21.5	19.49	19.01	18.82	0.026	0.023	0.024	
155	05:39:57.75	-69:45:10.1	19.26	17.88	17.00	0.020	0.010	0.009	
156	05:39:57.77	-69:44:15.3	17.77	17.55	17.46	0.007	0.008	0.009	
157	05:39:57.78	-69:44:55.3	15.60	15.31	15.20	0.004	0.002	0.003	
158	05:39:57.80	-69:43:31.8	19.03	19.17	18.98	0.032	0.034	0.037	
160	05:39:57.82	-69:44:12.6	17.44	16.88	16.58	0.008	0.005	0.005	
161	05:39:57.82	-69:45:03.3	18.96	17.91	17.32	0.015	0.013	0.011	
162	05:39:57.83	-69:43:47.7	14.93	14.10	13.98	0.005	0.002	0.002	
163	05:39:57.83	-69:45:33.9	16.34	16.18	16.17	0.006	0.005	0.009	
164	05:39:57.88	-69:43:45.0	18.53	17.68	17.55	0.014	0.013	0.013	
165	05:39:57.88	-69:44:44.4	16.76	16.54	16.40	0.007	0.014	0.027	
166	05:39:57.92	-69:44:26.1	18.60	17.65	17.38	0.015	0.010	0.017	
167	05:39:57.96	-69:44:08.8	18.67	17.73	17.41	0.015	0.009	0.010	
168	05:39:58.04	-69:44:54.0	15.91	15.19	15.02	0.005	0.003	0.003	
169	05:39:58.06	-69:44:38.3	18.59	18.42	18.29	0.016	0.022	0.023	
170	05:39:58.08	-69:43:54.6	17.83	17.22	17.10	0.008	0.007	0.009	
171	05:39:58.13	-69:43:35.6	17.92	17.37	17.27	0.011	0.008	0.010	
172	05:39:58.16	-69:43:49.2	19.59	18.56	18.33	0.032	0.025	0.030	

Table 1. continued...

ID	RA (J 2000.0)	DEC (J 2000.0)	J (mag)	H (mag)	Ks (mag)	σJ	σH	σKs	notes
173	05:39:58.18	-69:45:31.9	16.40	14.85	14.26	0.004	0.003	0.004	
174	05:39:58.18	-69:45:37.4	17.00	16.16	15.80	0.008	0.004	0.005	
175	05:39:58.21	-69:44:22.5	18.54	18.41	18.33	0.015	0.018	0.022	
176	05:39:58.26	-69:43:40.9	18.63	18.27	18.08	0.013	0.017	0.018	
177	05:39:58.26	-69:44:31.0	19.23	18.99	18.91	0.021	0.025	0.034	
179	05:39:58.31	-69:43:38.4	17.07	16.00	15.77	0.009	0.003	0.005	
180	05:39:58.46	-69:43:50.9	18.99	18.69	18.66	0.022	0.023	0.029	
181	05:39:58.47	-69:44:07.1	17.88	17.51	17.34	0.013	0.009	0.008	
182	05:39:58.49	-69:43:32.6	17.75	17.37	17.14	0.009	0.011	0.011	
183	05:39:58.48	-69:45:23.7	18.30	17.70	17.59	0.012	0.010	0.014	
184	05:39:58.51	-69:45:25.5	19.93	19.07	18.70	0.041	0.032	0.028	
185	05:39:58.53	-69:45:15.3	17.64	16.85	16.49	0.010	0.023	0.032	
186	05:39:58.56	-69:44:30.7	18.93	18.40	18.25	0.015	0.016	0.021	
187	05:39:58.60	-69:44:34.8	17.20	16.63	16.50	0.005	0.005	0.005	
188	05:39:58.64	-69:43:57.4	19.45	18.29	17.92	0.026	0.016	0.013	
189	05:39:58.65	-69:44:41.8	15.14	14.92	14.76	0.005	0.002	0.003	
190	05:39:58.71	-69:43:48.2	18.49	17.63	17.35	0.014	0.012	0.012	
191	05:39:58.71	-69:44:38.3	13.85	12.98	12.78	0.004	0.002	0.002	
192	05:39:58.75	-69:44:10.0	16.00	15.76	15.66	0.005	0.002	0.003	
193	05:39:58.76	-69:44:04.0	12.69	12.68	12.70	0.003	0.002	0.002	R 149, Sk−69°257
194	05:39:58.78	-69:45:18.9	18.03	17.91	17.97	0.009	0.011	0.021	
196	05:39:58.82	-69:45:17.1	17.77	17.22	17.12	0.010	0.008	0.012	
197	05:39:58.83	-69:43:55.4	18.77	18.05	17.73	0.017	0.012	0.013	
198	05:39:58.86	-69:43:36.1	17.78	17.11	17.01	0.008	0.007	0.009	
199	05:39:58.92	-69:45:31.5	15.19	14.53	14.31	0.003	0.002	0.005	
200	05:39:58.92	-69:44:49.3	17.83	17.25	17.13	0.008	0.006	0.008	
201	05:39:58.97	-69:43:51.9	14.75	14.50	14.43	0.005	0.002	0.003	
202	05:39:58.97	-69:44:53.4	18.66	18.40	18.17	0.014	0.024	0.021	
203	05:39:58.97	-69:45:09.3	19.50	18.88	18.43	0.028	0.024	0.023	
204	05:39:59.17	-69:43:34.1	19.28	18.52	17.83	0.035	0.036	0.042	
205	05:39:59.27	-69:44:31.2	18.49	17.99	17.83	0.013	0.010	0.012	
206	05:39:59.31	-69:43:57.8	14.94	14.90	14.96	0.004	0.002	0.003	
207	05:39:59.34	-69:45:35.9	19.44	18.81	18.80	0.024	0.035	0.032	
209	05:39:59.39	-69:43:38.7	17.74	17.13	17.08	0.007	0.007	0.012	
210	05:39:59.41	-69:45:26.1	16.49	13.87	11.79	0.005	0.002	0.002	
211	05:39:59.44	-69:45:00.7	19.10	18.27	18.19	0.022	0.018	0.023	
212	05:39:59.45	-69:44:27.4	18.42	17.48	17.15	0.014	0.009	0.008	
214	05:39:59.52	-69:44:17.6	16.37	15.75	15.61	0.005	0.003	0.004	
215	05:39:59.57	-69:44:06.2	17.23	16.31	15.99	0.009	0.007	0.005	
216	05:39:59.58	-69:44:58.0	18.49	17.88	17.72	0.013	0.017	0.016	
217	05:39:59.58	-69:45:32.4	18.48	17.77	17.50	0.018	0.011	0.012	
218	05:39:59.62	-69:44:44.9	17.67	17.46	17.35	0.008	0.008	0.011	
219	05:39:59.69	-69:44:53.3	18.30	17.89	17.49	0.016	0.016	0.014	
220	05:39:59.69	-69:45:37.2	19.62	18.69	18.42	0.028	0.022	0.025	
221	05:39:59.73	-69:44:34.9	18.51	18.35	18.19	0.013	0.017	0.016	
222	05:39:59.74	-69:44:08.1	19.09	18.59	18.04	0.022	0.019	0.014	
223	05:39:59.76	-69:45:04.0	17.54	16.88	16.74	0.007	0.005	0.005	
224	05:39:59.77	-69:45:26.9	18.79	17.60	18.34	0.018	0.011	0.039	
225	05:39:59.80	-69:45:30.8	18.21	17.43	17.27	0.010	0.010	0.013	
226	05:39:59.83	-69:44:50.0	17.27	16.73	16.63	0.006	0.005	0.007	
227	05:39:59.84	-69:44:39.7	18.67	18.43	18.40	0.015	0.021	0.026	
228	05:39:59.85	-69:45:22.1	16.80	15.63	14.81	0.006	0.003	0.004	
229	05:39:59.86	-69:43:57.3	17.29	16.64	16.51	0.006	0.005	0.007	
230	05:39:59.87	-69:44:12.8	18.20	17.88	17.86	0.010	0.013	0.017	

Table 1. continued...

ID	RA (J 2000.0)	DEC (J 2000.0)	*J* (mag)	*H* (mag)	*Ks* (mag)	σ*J*	σ*H*	σ*Ks*	notes
231	05:39:59.87	-69:44:02.7	18.43	18.21	18.08	0.011	0.015	0.018	
232	05:39:59.91	-69:44:55.4	15.86	14.47	13.93	0.004	0.002	0.003	
233	05:39:59.91	-69:44:36.1	17.72	17.44	17.23	0.008	0.008	0.009	
235	05:39:59.94	-69:44:16.8	19.25	18.72	18.45	0.030	0.023	0.020	
236	05:40:00.02	-69:43:35.4	18.26	17.55	17.26	0.013	0.014	0.016	
238	05:40:00.07	-69:43:47.6	18.84	18.11	17.86	0.017	0.014	0.013	
239	05:40:00.12	-69:45:30.0	17.32	16.63	16.52	0.006	0.005	0.007	
240	05:40:00.14	-69:45:17.1	17.53	16.96	16.87	0.007	0.007	0.009	
241	05:40:00.19	-69:43:45.9	19.27	19.19	19.18	0.026	0.034	0.044	
242	05:40:00.19	-69:44:51.9	17.84	17.45	17.36	0.009	0.013	0.009	
243	05:40:00.19	-69:45:41.5	16.46	15.96	15.85	0.005	0.007	0.008	
245	05:40:00.22	-69:45:16.0	17.66	17.05	16.73	0.008	0.008	0.007	
246	05:40:00.24	-69:44:42.8	16.64	15.93	15.56	0.005	0.004	0.004	
247	05:40:00.29	-69:44:31.2	19.12	18.16	17.75	0.020	0.010	0.013	
250	05:40:00.47	-69:45:07.0	19.77	18.91	18.53	0.029	0.024	0.023	
251	05:40:00.47	-69:45:40.9	16.89	16.35	16.30	0.009	0.007	0.010	
253	05:40:00.54	-69:43:52.4	19.24	18.45	18.29	0.020	0.015	0.018	
254	05:40:00.55	-69:45:17.1	17.12	16.54	16.26	0.005	0.005	0.006	
255	05:40:00.57	-69:45:11.5	19.67	18.79	18.31	0.028	0.023	0.019	
256	05:40:00.70	-69:43:47.9	17.75	17.66	17.64	0.008	0.011	0.014	
257	05:40:00.70	-69:44:58.9	17.65	17.06	16.96	0.010	0.006	0.006	
258	05:40:00.72	-69:44:16.8	19.10	18.67	18.70	0.027	0.023	0.035	
259	05:40:00.72	-69:44:56.6	18.89	18.06	17.73	0.019	0.011	0.012	
260	05:40:00.75	-69:45:30.7	17.76	16.53	16.06	0.008	0.006	0.005	
261	05:40:00.81	-69:44:24.9	18.05	17.75	17.60	0.010	0.012	0.012	
262	05:40:00.81	-69:43:42.0	17.30	16.70	16.62	0.009	0.005	0.009	
263	05:40:00.82	-69:45:00.9	15.78	15.07	14.88	0.004	0.003	0.004	
264	05:40:00.82	-69:45:09.1	18.44	17.60	17.16	0.013	0.009	0.008	
265	05:40:00.86	-69:44:14.4	14.46	13.18	12.72	0.006	0.001	0.002	
266	05:40:00.90	-69:44:39.4	18.73	18.24	18.04	0.018	0.015	0.023	
267	05:40:00.90	-69:44:36.7	16.36	15.79	15.65	0.005	0.003	0.003	
268	05:40:00.92	-69:44:03.7	17.76	17.29	17.21	0.007	0.007	0.008	
269	05:40:00.97	-69:44:21.9	18.24	17.71	17.59	0.010	0.009	0.009	
270	05:40:01.00	-69:45:24.6	17.40	16.93	16.81	0.007	0.006	0.006	
271	05:40:01.09	-69:44:07.9	16.75	16.43	16.33	0.014	0.008	0.007	
272	05:40:01.11	-69:45:31.2	17.78	17.08	16.82	0.012	0.010	0.009	
273	05:40:01.11	-69:45:10.1	19.26	18.07	16.96	0.025	0.024	0.017	
274	05:40:01.14	-69:44:46.1	19.34	19.06	18.93	0.021	0.031	0.032	
275	05:40:01.14	-69:44:58.3	17.11	16.59	16.34	0.008	0.004	0.005	
276	05:40:01.15	-69:45:11.5	19.40	18.81	18.51	0.022	0.023	0.025	
278	05:40:01.23	-69:44:58.9	16.97	16.50	16.24	0.008	0.005	0.005	
279	05:40:01.26	-69:44:03.5	16.20	15.49	15.35	0.005	0.003	0.004	
280	05:40:01.35	-69:45:17.8	17.94	16.36	15.78	0.010	0.006	0.007	
281	05:40:01.42	-69:44:49.8	17.51	17.26	17.15	0.006	0.007	0.008	
282	05:40:01.49	-69:44:39.5	19.31	18.80	18.54	0.028	0.021	0.025	
283	05:40:01.54	-69:44:31.4	18.78	18.23	17.93	0.015	0.013	0.014	
284	05:40:01.57	-69:44:51.0	18.45	17.83	17.44	0.017	0.020	0.022	
285	05:40:01.57	-69:45:01.1	17.67	17.10	16.78	0.007	0.007	0.007	
286	05:40:01.64	-69:43:50.3	17.34	16.38	16.07	0.007	0.006	0.006	
287	05:40:01.68	-69:44:37.8	15.95	14.78	14.35	0.006	0.002	0.002	
288	05:40:01.73	-69:44:41.8	19.93	18.93	18.27	0.049	0.023	0.020	
289	05:40:01.76	-69:45:20.0	17.71	17.09	16.80	0.008	0.006	0.006	
290	05:40:01.77	-69:43:46.6	12.90	11.91	11.66	0.002	0.001	0.001	
291	05:40:01.82	-69:44:16.0	18.39	17.64	17.35	0.011	0.010	0.009	
292	05:40:01.85	-69:44:39.2	16.88	16.52	16.37	0.006	0.004	0.007	

Table 1. continued...

ID	RA (J 2000.0)	DEC (J 2000.0)	J (mag)	H (mag)	Ks (mag)	σJ	σH	σKs	notes
293	05:40:01.89	-69:45:39.8	18.68	18.17	18.15	0.016	0.015	0.023	
294	05:40:01.90	-69:45:28.2	18.03	17.39	17.32	0.009	0.007	0.013	
295	05:40:01.91	-69:44:55.9	19.48	18.33	17.62	0.034	0.017	0.019	
298	05:40:02.04	-69:43:43.4	17.37	16.84	16.75	0.009	0.008	0.008	
299	05:40:02.07	-69:45:13.4	17.82	16.55	16.10	0.008	0.004	0.005	
300	05:40:02.10	-69:44:15.1	16.49	16.49	16.52	0.005	0.004	0.005	
301	05:40:02.13	-69:44:47.5	17.98	17.60	17.50	0.011	0.010	0.014	
302	05:40:02.18	-69:45:18.4	18.43	17.11	16.62	0.011	0.008	0.007	
303	05:40:02.18	-69:45:01.6	18.08	16.43	15.68	0.010	0.004	0.004	
304	05:40:02.20	-69:44:36.6	18.95	18.17	17.69	0.022	0.013	0.013	
305	05:40:02.21	-69:44:50.5	19.42	18.81	18.61	0.028	0.031	0.027	
306	05:40:02.24	-69:44:08.0	18.82	18.28	18.16	0.015	0.015	0.019	
307	05:40:02.26	-69:44:12.1	17.60	17.27	17.45	0.016	0.033	0.011	
308	05:40:02.27	-69:44:22.6	19.71	18.57	18.04	0.028	0.018	0.015	
310	05:40:02.34	-69:45:35.9	18.04	17.38	17.20	0.011	0.009	0.008	
311	05:40:02.37	-69:44:42.0	17.70	17.59	17.51	0.009	0.013	0.011	
312	05:40:02.42	-69:44:19.9	19.03	18.27	17.90	0.018	0.013	0.014	
313	05:40:02.45	-69:44:46.4	15.08	14.84	14.61	0.003	0.002	0.002	
314	05:40:02.46	-69:44:27.1	19.93	18.84	18.51	0.038	0.021	0.029	
315	05:40:02.54	-69:44:55.3	19.29	18.26	17.75	0.024	0.012	0.012	
316	05:40:02.56	-69:43:48.9	17.39	16.68	16.42	0.009	0.006	0.008	
317	05:40:02.77	-69:44:07.4	17.94	17.38	17.25	0.008	0.007	0.008	
317.1	05:40:02.77	-69:44:59.3	> 20	18.14	16.32	–	–	–	
318	05:40:02.81	-69:44:38.9	17.07	16.85	16.75	0.011	0.008	0.013	
319	05:40:02.86	-69:43:54.5	18.11	17.86	17.82	0.010	0.021	0.037	
320	05:40:02.88	-69:44:44.4	19.23	18.89	18.58	0.035	0.038	0.043	
321	05:40:02.88	-69:45:34.3	18.80	18.54	18.53	0.015	0.017	0.025	
322	05:40:02.99	-69:44:32.5	19.43	18.61	18.28	0.026	0.018	0.019	
324	05:40:03.08	-69:43:52.1	17.47	17.38	17.39	0.006	0.009	0.012	
325	05:40:03.15	-69:43:53.6	18.81	18.45	18.31	0.017	0.027	0.041	
326	05:40:03.15	-69:45:10.4	19.02	18.14	17.67	0.019	0.014	0.014	
327	05:40:03.15	-69:44:22.5	19.27	18.09	17.61	0.021	0.011	0.012	
328	05:40:03.16	-69:45:39.0	18.72	18.47	18.28	0.013	0.017	0.020	
330	05:40:03.20	-69:44:29.1	18.73	18.49	18.31	0.016	0.022	0.029	
331	05:40:03.22	-69:44:26.3	19.19	17.99	17.56	0.021	0.012	0.011	
332	05:40:03.28	-69:44:42.8	19.03	18.62	18.36	0.018	0.034	0.042	
333	05:40:03.32	-69:45:20.9	18.35	17.84	17.85	0.017	0.008	0.014	
334	05:40:03.33	-69:44:50.8	18.22	17.67	17.41	0.013	0.011	0.009	
335	05:40:03.34	-69:44:35.9	19.12	18.33	17.76	0.026	0.017	0.016	
336	05:40:03.37	-69:44:17.0	19.14	18.34	18.02	0.022	0.019	0.019	
337	05:40:03.40	-69:45:33.2	19.58	19.19	18.98	0.035	0.034	0.034	
338	05:40:03.42	-69:44:38.2	19.47	19.08	18.65	0.034	0.035	0.028	
339	05:40:03.45	-69:43:52.6	16.03	15.30	15.09	0.005	0.004	0.005	
340	05:40:03.51	-69:44:42.9	19.00	18.24	17.70	0.024	0.023	0.019	
341	05:40:03.52	-69:44:46.8	17.89	17.29	17.14	0.008	0.009	0.009	
342	05:40:03.55	-69:43:39.2	17.97	17.67	17.58	0.013	0.011	0.016	
343	05:40:03.58	-69:43:55.8	19.10	17.63	16.73	0.028	0.029	0.035	
344	05:40:03.62	-69:45:39.2	18.31	17.25	16.93	0.011	0.007	0.009	
345	05:40:03.64	-69:43:37.2	18.79	17.76	17.40	0.016	0.009	0.014	
346	05:40:03.64	-69:44:54.7	17.31	16.71	16.58	0.007	0.006	0.007	
347	05:40:03.65	-69:45:41.6	18.74	18.05	17.81	0.019	0.015	0.014	
348	05:40:03.66	-69:44:49.7	15.92	15.61	15.31	0.005	0.002	0.003	
349	05:40:03.67	-69:44:19.2	17.63	17.08	16.96	0.008	0.007	0.009	
350	05:40:03.77	-69:44:36.0	17.81	17.28	17.15	0.011	0.011	0.014	
351	05:40:03.77	-69:45:00.8	18.99	17.74	17.21	0.020	0.009	0.007	

continued...

Table 1. continued...

ID	RA (J 2000.0)	DEC (J 2000.0)	J (mag)	H (mag)	Ks (mag)	σJ	σH	σKs	notes
352	05:40:03.79	-69:45:20.0	19.72	19.00	18.81	0.031	0.036	0.029	
353	05:40:03.80	-69:44:33.0	17.51	16.54	15.52	0.008	0.004	0.004	
354	05:40:03.82	-69:43:36.0	19.14	18.59	18.44	0.030	0.018	0.022	
355	05:40:03.82	-69:43:44.4	19.24	18.29	18.03	0.024	0.016	0.017	
356	05:40:03.88	-69:45:29.7	19.06	18.75	18.64	0.027	0.029	0.030	
357	05:40:03.89	-69:45:32.1	16.19	16.05	16.03	0.006	0.004	0.004	
358	05:40:03.89	-69:45:10.8	18.72	18.11	17.89	0.017	0.018	0.026	
359	05:40:04.00	-69:44:07.7	16.49	15.83	15.66	0.005	0.004	0.005	
360	05:40:04.05	-69:44:47.2	18.11	17.13	16.54	0.010	0.008	0.007	
361	05:40:04.09	-69:43:51.8	14.47	14.40	14.43	0.004	0.004	0.007	
362	05:40:04.09	-69:43:55.5	18.29	18.27	18.21	0.012	0.017	0.019	
363	05:40:04.11	-69:43:36.7	18.97	18.67	18.70	0.024	0.026	0.030	
364	05:40:04.12	-69:45:03.7	16.76	16.28	16.30	0.015	0.026	0.007	
365	05:40:04.14	-69:44:58.5	16.93	14.83	13.86	0.006	0.003	0.003	
366	05:40:04.23	-69:43:49.3	19.45	18.88	18.79	0.038	0.024	0.024	
367	05:40:04.25	-69:45:18.9	19.07	18.44	18.32	0.025	0.015	0.017	
368	05:40:04.26	-69:45:29.8	19.55	19.11	18.90	0.044	0.034	0.034	
369	05:40:04.34	-69:44:03.4	18.49	17.61	17.32	0.014	0.009	0.013	
370	05:40:04.35	-69:45:05.4	17.43	16.99	16.67	0.008	0.007	0.008	
371	05:40:04.46	-69:44:37.4	15.13	14.67	14.30	0.000	0.000	0.000	Main source in Papillon nebula
372	05:40:04.46	-69:45:21.0	19.33	18.87	18.77	0.027	0.024	0.033	
373	05:40:04.50	-69:45:22.1	18.85	18.77	18.74	0.020	0.019	0.026	
375	05:40:04.52	-69:45:07.3	17.58	16.99	16.87	0.006	0.006	0.009	
376	05:40:04.57	-69:43:54.1	19.95	19.19	18.84	0.035	0.030	0.029	
377	05:40:04.57	-69:43:57.6	18.97	18.43	18.18	0.017	0.017	0.018	
378	05:40:04.60	-69:43:41.8	18.46	17.48	17.20	0.012	0.012	0.018	
379	05:40:04.63	-69:44:15.0	16.87	16.41	16.28	0.005	0.003	0.005	
380	05:40:04.66	-69:43:34.3	19.08	19.00	18.89	0.024	0.029	0.030	
381	05:40:04.68	-69:45:00.7	17.34	16.77	16.48	0.006	0.005	0.005	
382	05:40:04.69	-69:44:26.9	19.63	18.09	17.42	0.033	0.011	0.012	
383	05:40:04.70	-69:44:51.3	19.82	18.83	18.29	0.035	0.031	0.029	
384	05:40:04.74	-69:44:07.8	18.87	17.81	17.43	0.017	0.010	0.011	
386	05:40:04.89	-69:45:23.6	18.21	17.32	17.11	0.012	0.009	0.011	
387	05:40:04.92	-69:45:28.8	16.30	16.18	16.17	0.007	0.004	0.005	
388	05:40:04.99	-69:45:14.4	19.09	18.27	17.89	0.019	0.017	0.013	
389	05:40:04.99	-69:45:36.9	16.11	16.07	16.11	0.007	0.006	0.007	
390	05:40:05.01	-69:44:23.2	17.79	17.23	17.09	0.009	0.006	0.008	
391	05:40:05.02	-69:43:54.0	17.95	17.90	17.89	0.010	0.011	0.016	
392	05:40:05.07	-69:44:11.3	17.62	17.04	16.90	0.007	0.008	0.008	
393	05:40:05.08	-69:43:51.3	18.53	18.35	18.33	0.014	0.021	0.028	
394	05:40:05.10	-69:43:40.2	17.87	16.96	16.68	0.009	0.009	0.015	
395	05:40:05.10	-69:44:55.6	19.49	18.42	17.75	0.030	0.020	0.014	
396	05:40:05.18	-69:45:03.5	16.65	16.24	15.93	0.007	0.004	0.006	
397	05:40:05.19	-69:44:34.7	17.75	17.23	17.03	0.014	0.011	0.010	
398	05:40:05.24	-69:45:23.6	16.66	16.48	16.44	0.005	0.006	0.005	
399	05:40:05.31	-69:44:23.6	19.19	17.89	17.28	0.021	0.013	0.016	
400	05:40:05.34	-69:45:20.6	18.33	18.01	17.99	0.012	0.014	0.015	
402	05:40:05.37	-69:45:04.3	18.62	18.18	17.92	0.034	0.039	0.035	
403	05:40:05.41	-69:43:32.5	18.59	17.96	17.48	0.019	0.015	0.020	
404	05:40:05.42	-69:44:44.0	14.09	13.17	12.91	0.004	0.001	0.002	
405	05:40:05.46	-69:44:37.7	19.02	18.56	18.19	0.026	0.031	0.041	
406	05:40:05.49	-69:43:37.7	19.71	19.07	18.96	0.038	0.025	0.039	
407	05:40:05.51	-69:44:40.8	18.49	17.56	16.84	0.019	0.013	0.010	
408	05:40:05.54	-69:44:11.0	16.72	16.24	16.04	0.011	0.005	0.004	

Table 1. continued...

ID	RA (J 2000.0)	DEC (J 2000.0)	J (mag)	H (mag)	Ks (mag)	σJ	σH	σKs	notes
409	05:40:05.56	-69:43:41.5	16.56	15.80	15.66	0.007	0.007	0.012	
410	05:40:05.68	-69:45:01.9	13.82	13.34	13.02	0.000	0.007	0.009	
411	05:40:05.70	-69:45:21.6	19.77	18.90	18.76	0.032	0.033	0.040	
412	05:40:05.71	-69:44:29.0	17.82	16.64	16.12	0.008	0.005	0.005	
413	05:40:05.72	-69:45:16.3	19.31	18.99	18.69	0.027	0.036	0.031	
414	05:40:05.77	-69:44:51.5	19.83	19.02	18.44	0.042	0.034	0.050	
415	05:40:05.79	-69:43:50.2	18.24	18.25	18.13	0.013	0.018	0.021	
416	05:40:05.79	-69:44:54.8	19.98	19.15	18.63	0.053	0.035	0.042	
417	05:40:05.82	-69:45:05.3	15.53	15.59	15.43	0.000	0.003	0.004	
418	05:40:05.86	-69:44:25.2	15.73	15.69	15.67	0.005	0.003	0.004	
419	05:40:05.88	-69:44:04.2	18.02	17.50	17.37	0.009	0.009	0.010	
420	05:40:05.90	-69:45:25.3	18.59	17.69	17.35	0.014	0.009	0.010	
421	05:40:05.92	-69:45:04.8	16.04	15.57	15.39	0.000	0.004	0.004	
422	05:40:05.94	-69:45:01.4	16.73	16.03	15.58	0.000	0.013	0.019	
423	05:40:05.94	-69:44:58.2	19.82	19.13	18.62	0.041	0.027	0.033	
424	05:40:05.95	-69:44:44.8	19.63	18.29	17.47	0.033	0.016	0.021	
425	05:40:05.98	-69:43:32.1	17.70	17.77	17.61	0.010	0.014	0.020	
426	05:40:05.98	-69:45:06.4	15.44	15.21	15.07	0.000	0.009	0.008	
427	05:40:05.99	-69:44:35.4	16.57	16.06	15.73	0.005	0.004	0.005	
428	05:40:06.05	-69:44:38.5	19.12	18.31	17.71	0.024	0.016	0.014	
429	05:40:06.07	-69:43:53.4	15.67	14.54	14.16	0.005	0.004	0.009	
430	05:40:06.06	-69:45:08.8	18.94	18.52	18.27	0.020	0.022	0.029	
432	05:40:06.11	-69:44:29.4	17.12	16.84	16.68	0.008	0.004	0.007	
433	05:40:06.12	-69:43:33.6	17.95	17.48	17.30	0.012	0.016	0.020	
434	05:40:06.19	-69:44:41.2	18.49	17.78	17.34	0.016	0.014	0.010	
435	05:40:06.18	-69:45:25.5	19.26	18.81	18.59	0.023	0.035	0.046	
436	05:40:06.20	-69:45:04.3	16.89	16.27	16.00	0.008	0.006	0.006	
439	05:40:06.37	-69:45:10.1	18.13	17.83	17.65	0.009	0.010	0.013	
440	05:40:06.40	-69:44:34.2	18.14	17.34	16.51	0.010	0.007	0.006	
441	05:40:06.41	-69:43:57.4	18.54	17.63	17.30	0.012	0.014	0.018	
442	05:40:06.45	-69:43:42.0	18.88	17.74	17.40	0.017	0.013	0.018	
443	05:40:06.50	-69:44:04.2	16.44	15.81	15.67	0.005	0.005	0.007	
444	05:40:06.51	-69:45:02.4	14.31	13.57	13.34	0.005	0.002	0.002	
445	05:40:06.61	-69:44:28.8	19.54	19.03	18.83	0.032	0.034	0.043	
446	05:40:06.65	-69:43:34.7	18.97	18.73	18.73	0.017	0.022	0.031	
447	05:40:06.70	-69:45:18.2	17.20	16.98	16.88	0.006	0.006	0.006	
448	05:40:06.74	-69:45:11.6	19.36	18.70	18.07	0.025	0.022	0.019	
449	05:40:06.74	-69:45:36.7	16.66	15.90	15.75	0.006	0.003	0.003	
450	05:40:06.78	-69:44:22.8	14.26	13.46	13.25	0.004	0.002	0.003	
451	05:40:06.79	-69:45:31.9	19.39	18.82	17.93	0.036	0.040	0.054	
452	05:40:06.80	-69:45:34.0	18.79	18.04	17.74	0.019	0.018	0.016	
453	05:40:06.80	-69:44:58.0	19.80	19.06	18.90	0.035	0.033	0.035	
454	05:40:06.85	-69:43:47.5	19.23	18.62	18.50	0.019	0.023	0.034	
455	05:40:06.85	-69:44:40.4	19.73	18.54	17.98	0.035	0.020	0.016	
456	05:40:06.85	-69:44:08.7	19.90	18.97	18.66	0.038	0.025	0.025	
457	05:40:06.87	-69:44:38.5	19.39	18.03	17.03	0.027	0.030	0.031	
458	05:40:06.90	-69:43:43.5	18.17	17.52	17.40	0.011	0.014	0.018	
459	05:40:06.89	-69:44:43.3	18.39	16.87	16.21	0.013	0.006	0.009	
460	05:40:06.91	-69:44:02.2	18.35	17.36	17.02	0.012	0.010	0.011	
461	05:40:06.94	-69:44:52.1	18.60	17.52	16.89	0.015	0.008	0.010	
462	05:40:06.96	-69:45:26.1	17.21	16.70	16.29	0.007	0.004	0.004	
463	05:40:06.97	-69:45:06.5	17.92	17.41	17.27	0.010	0.007	0.008	
464	05:40:06.98	-69:44:05.5	19.39	18.38	18.05	0.022	0.019	0.021	
465	05:40:07.02	-69:45:23.5	19.76	18.89	18.70	0.041	0.034	0.034	
466	05:40:07.03	-69:43:58.2	17.07	16.47	16.31	0.007	0.007	0.009	

Table 1. continued...

ID	RA (J 2000.0)	DEC (J 2000.0)	J (mag)	H (mag)	Ks (mag)	σJ	σH	σKs	notes
467	05:40:07.07	-69:44:40.6	19.14	18.66	18.43	0.024	0.020	0.020	
468	05:40:07.21	-69:44:29.9	19.61	18.41	17.64	0.029	0.017	0.018	
469	05:40:07.21	-69:44:55.4	19.24	18.09	17.49	0.023	0.014	0.010	
470	05:40:07.33	-69:44:08.6	18.35	17.47	17.15	0.012	0.011	0.013	
471	05:40:07.41	-69:44:53.8	19.17	18.55	17.99	0.022	0.022	0.023	
472	05:40:07.42	-69:43:57.2	18.21	18.06	17.97	0.012	0.012	0.014	
473	05:40:07.47	-69:45:37.0	13.96	13.11	12.92	0.002	0.002	0.002	
474	05:40:07.52	-69:43:53.6	19.58	19.17	18.74	0.026	0.031	0.030	
475	05:40:07.60	-69:45:26.3	15.43	15.33	15.32	0.008	0.009	0.004	
476	05:40:07.63	-69:45:27.7	18.23	17.98	17.94	0.014	0.019	0.014	
477	05:40:07.71	-69:45:04.9	19.30	18.99	18.77	0.022	0.026	0.031	
478	05:40:07.79	-69:44:02.5	18.60	18.43	18.28	0.014	0.019	0.024	
479	05:40:07.81	-69:44:20.3	18.95	18.42	18.31	0.019	0.016	0.021	
480	05:40:07.89	-69:43:42.7	19.16	18.25	17.93	0.020	0.017	0.021	
481	05:40:07.90	-69:43:59.6	18.61	18.05	17.83	0.022	0.018	0.018	
482	05:40:07.93	-69:43:49.4	17.96	17.32	17.23	0.010	0.012	0.019	
483	05:40:07.95	-69:45:18.4	18.69	18.12	17.63	0.019	0.012	0.011	
484	05:40:07.96	-69:45:01.0	17.67	16.66	16.18	0.010	0.005	0.005	
485	05:40:07.97	-69:44:10.3	18.70	18.10	17.96	0.016	0.011	0.018	
487	05:40:08.01	-69:45:11.4	17.96	17.67	17.57	0.008	0.011	0.014	
488	05:40:08.10	-69:45:20.0	19.74	19.19	19.23	0.032	0.042	0.064	
489	05:40:08.10	-69:45:15.6	18.87	18.44	17.89	0.019	0.022	0.024	
490	05:40:08.13	-69:43:40.6	17.89	17.22	17.15	0.009	0.013	0.020	
491	05:40:08.20	-69:45:09.8	19.51	19.37	19.03	0.039	0.035	0.046	
492	05:40:08.22	-69:45:32.2	18.68	17.95	17.65	0.017	0.017	0.015	
493	05:40:08.23	-69:44:55.8	17.57	16.87	16.70	0.008	0.007	0.010	
494	05:40:08.30	-69:45:04.7	19.64	18.90	18.65	0.034	0.028	0.036	
495	05:40:08.35	-69:43:35.5	15.83	15.09	14.94	0.006	0.011	0.018	
496	05:40:08.36	-69:45:12.8	17.34	16.27	15.91	0.008	0.003	0.005	
497	05:40:08.46	-69:44:05.4	17.40	16.86	16.75	0.008	0.009	0.011	
499	05:40:08.70	-69:44:51.2	14.01	13.13	12.90	0.002	0.003	0.003	
500	05:40:08.76	-69:44:54.7	17.99	17.83	17.66	0.008	0.012	0.012	
501	05:40:08.82	-69:45:21.5	17.39	16.52	16.20	0.012	0.006	0.008	
502	05:40:08.83	-69:45:32.4	16.28	16.08	16.06	0.008	0.008	0.013	
503	05:40:08.88	-69:44:59.8	19.53	19.02	18.65	0.025	0.035	0.032	
504	05:40:08.90	-69:44:21.4	18.31	17.78	17.47	0.013	0.011	0.012	
505	05:40:08.93	-69:45:14.1	17.92	17.49	17.33	0.012	0.008	0.012	
506	05:40:08.99	-69:45:02.2	18.49	17.32	16.80	0.013	0.008	0.006	
507	05:40:09.00	-69:45:27.6	18.57	18.60	18.56	0.026	0.043	0.070	
508	05:40:09.01	-69:45:31.5	16.05	15.84	15.79	0.007	0.009	0.019	
509	05:40:09.29	-69:44:35.2	17.90	17.33	17.13	0.011	0.009	0.013	
510	05:40:09.32	-69:45:13.5	18.78	18.43	18.18	0.018	0.020	0.032	
512	05:40:09.35	-69:44:41.3	16.64	15.99	15.81	0.005	0.004	0.005	
513	05:40:09.35	-69:44:15.6	16.93	16.40	16.27	0.006	0.006	0.009	
514	05:40:09.36	-69:45:20.6	18.81	18.45	17.68	0.020	0.019	0.016	
515	05:40:09.37	-69:45:40.5	18.32	17.64	17.51	0.014	0.010	0.012	
516	05:40:09.41	-69:45:12.5	18.30	17.97	17.92	0.013	0.013	0.021	
517	05:40:09.44	-69:44:52.9	19.26	18.33	17.78	0.029	0.053	0.059	
518	05:40:09.71	-69:45:19.1	19.83	19.03	18.24	0.047	0.032	0.018	
519	05:40:09.72	-69:45:27.1	19.07	18.72	18.65	0.020	0.023	0.030	
520	05:40:09.73	-69:44:14.1	18.57	17.67	17.28	0.016	0.010	0.014	
521	05:40:09.75	-69:45:41.6	17.17	16.54	16.42	0.012	0.017	0.021	
522	05:40:09.81	-69:43:57.9	18.44	17.51	17.19	0.015	0.018	0.018	
523	05:40:09.83	-69:45:01.3	18.38	17.64	17.51	0.012	0.011	0.010	
524	05:40:09.83	-69:45:08.8	18.99	18.77	18.54	0.021	0.026	0.030	

Table 1. continued...

ID	RA (J 2000.0)	DEC (J 2000.0)	J (mag)	H (mag)	Ks (mag)	σJ	σH	σKs	notes
525	05:40:09.84	-69:45:13.4	19.87	18.92	18.71	0.051	0.024	0.026	
526	05:40:09.89	-69:44:55.7	17.49	16.93	16.81	0.011	0.010	0.007	
527	05:40:09.90	-69:44:11.1	19.95	19.39	19.08	0.038	0.037	0.035	
528	05:40:10.15	-69:43:32.4	17.09	17.20	17.08	0.010	0.019	0.027	
529	05:40:10.26	-69:43:55.4	18.67	17.68	17.28	0.014	0.014	0.014	
530	05:40:10.27	-69:44:59.9	17.62	17.01	16.83	0.010	0.005	0.007	
531	05:40:10.34	-69:43:40.9	18.27	17.36	17.12	0.012	0.013	0.019	
532	05:40:10.37	-69:44:39.7	18.45	17.85	17.60	0.017	0.016	0.017	
533	05:40:10.41	-69:44:51.5	19.19	17.77	17.00	0.028	0.010	0.010	
534	05:40:10.53	-69:45:17.0	18.94	18.00	17.79	0.019	0.013	0.014	
535	05:40:10.55	-69:44:18.9	17.43	16.87	16.74	0.007	0.008	0.009	
536	05:40:10.56	-69:45:36.6	17.86	17.18	17.14	0.010	0.007	0.007	
537	05:40:10.60	-69:43:38.3	16.17	15.36	15.23	0.007	0.012	0.019	
538	05:40:10.65	-69:43:51.5	19.59	18.86	18.76	0.028	0.029	0.027	
539	05:40:10.68	-69:44:49.2	17.68	16.99	16.83	0.009	0.007	0.009	
541	05:40:10.79	-69:45:09.5	18.18	17.23	16.64	0.015	0.007	0.007	
542	05:40:11.04	-69:45:26.1	18.36	17.65	17.53	0.012	0.009	0.011	
543	05:40:11.16	-69:45:28.3	18.90	17.90	17.76	0.016	0.010	0.013	
544	05:40:11.22	-69:44:16.6	19.13	18.59	18.44	0.018	0.020	0.023	
545	05:40:11.23	-69:45:06.1	18.78	17.69	17.05	0.017	0.008	0.007	
546	05:40:11.27	-69:45:20.0	17.46	16.78	16.70	0.008	0.006	0.006	
547	05:40:11.34	-69:43:38.4	19.01	17.96	17.73	0.022	0.019	0.027	
548	05:40:11.34	-69:44:26.4	19.18	18.03	17.49	0.021	0.014	0.011	
549	05:40:11.36	-69:44:47.5	17.73	17.16	16.99	0.008	0.006	0.007	
550	05:40:11.44	-69:45:24.5	18.47	17.74	17.68	0.015	0.008	0.012	
551	05:40:11.49	-69:44:56.7	18.52	17.01	16.27	0.016	0.007	0.007	
552	05:40:11.52	-69:44:59.2	19.69	18.47	17.83	0.036	0.018	0.013	
553	05:40:11.57	-69:45:36.9	19.87	19.17	19.16	0.042	0.031	0.040	
554	05:40:11.60	-69:44:37.1	19.57	18.18	17.53	0.028	0.015	0.014	
555	05:40:11.65	-69:44:53.5	16.66	16.06	15.69	0.008	0.009	0.010	
556	05:40:11.67	-69:45:09.8	18.71	18.49	18.37	0.018	0.019	0.020	
557	05:40:11.73	-69:45:32.1	17.41	16.65	16.55	0.010	0.006	0.010	
558	05:40:11.74	-69:45:08.6	19.82	19.22	19.12	0.035	0.036	0.044	
559	05:40:11.81	-69:43:45.3	17.67	17.04	17.01	0.007	0.014	0.024	
560	05:40:11.87	-69:45:00.4	19.26	18.52	18.08	0.029	0.022	0.017	
561	05:40:11.91	-69:43:42.9	19.03	17.97	17.63	0.017	0.018	0.023	
562	05:40:11.93	-69:45:05.0	19.87	19.19	18.80	0.040	0.032	0.029	
563	05:40:11.96	-69:44:36.1	19.67	19.04	19.00	0.030	0.028	0.033	
564	05:40:11.99	-69:45:38.3	18.70	17.88	17.64	0.016	0.012	0.015	
565	05:40:12.06	-69:44:53.3	17.52	17.04	16.83	0.007	0.010	0.014	
566	05:40:12.06	-69:45:35.8	19.52	18.87	18.88	0.023	0.028	0.028	
567	05:40:12.23	-69:43:51.8	18.82	18.14	18.03	0.014	0.020	0.027	
568	05:40:12.32	-69:44:38.2	19.49	18.58	18.21	0.029	0.019	0.021	
569	05:40:12.34	-69:45:06.0	17.66	17.03	16.90	0.007	0.005	0.006	
570	05:40:12.38	-69:45:27.2	18.45	17.53	17.33	0.016	0.010	0.009	
571	05:40:12.47	-69:45:17.9	18.10	17.83	17.81	0.010	0.010	0.012	
572	05:40:12.51	-69:43:46.5	20.00	19.36	19.12	0.031	0.038	0.041	
573	05:40:12.64	-69:44:55.3	16.76	16.26	15.94	0.008	0.005	0.005	
574	05:40:12.64	-69:45:10.9	18.79	18.28	18.05	0.017	0.012	0.018	
575	05:40:12.66	-69:43:57.5	18.84	18.31	18.14	0.016	0.025	0.029	
576	05:40:12.68	-69:45:21.7	16.91	16.09	15.94	0.008	0.003	0.004	
577	05:40:12.78	-69:45:34.1	17.65	16.83	16.67	0.009	0.008	0.010	
578	05:40:12.82	-69:45:13.3	17.36	16.61	16.40	0.009	0.006	0.006	
579	05:40:12.90	-69:43:46.7	18.11	17.46	17.38	0.010	0.018	0.027	
580	05:40:12.98	-69:44:50.3	19.74	19.70	19.32	0.034	0.079	0.101	

Table 1. continued...

ID	RA (J 2000.0)	DEC (J 2000.0)	J (mag)	H (mag)	Ks (mag)	σJ	σH	σKs	notes
581	05:40:12.99	-69:44:09.2	18.12	17.46	17.17	0.010	0.013	0.015	
582	05:40:12.98	-69:45:29.5	17.54	16.77	16.67	0.011	0.007	0.010	
583	05:40:13.06	-69:44:58.0	18.40	17.91	17.77	0.010	0.019	0.030	
584	05:40:13.20	-69:45:23.4	18.09	17.24	17.09	0.014	0.007	0.007	
585	05:40:13.29	-69:45:18.1	19.48	18.59	18.40	0.022	0.019	0.020	
586	05:40:13.33	-69:43:54.5	18.94	18.70	18.50	0.028	0.036	0.031	
587	05:40:13.36	-69:45:11.8	18.24	17.57	17.46	0.012	0.008	0.011	
588	05:40:13.52	-69:43:50.6	12.20	11.49	11.36	0.001	0.001	0.001	
589	05:40:13.52	-69:45:29.4	15.77	14.78	14.57	0.008	0.006	0.010	
590	05:40:13.60	-69:44:08.9	16.01	15.26	15.12	0.007	0.009	0.014	
591	05:40:13.64	-69:45:36.0	19.50	18.74	18.38	0.031	0.029	0.023	
592	05:40:13.73	-69:44:47.0	14.60	14.05	13.73	0.004	0.005	0.005	
593	05:40:13.85	-69:44:23.2	18.64	18.07	17.98	0.015	0.016	0.021	
594	05:40:13.85	-69:45:10.4	19.05	18.64	18.47	0.024	0.018	0.024	
595	05:40:13.92	-69:44:02.6	19.92	18.77	18.51	0.041	0.028	0.033	
596	05:40:13.94	-69:44:00.2	19.15	18.26	17.95	0.019	0.021	0.024	
597	05:40:13.96	-69:45:08.7	19.12	18.95	18.79	0.023	0.025	0.034	
598	05:40:13.98	-69:44:53.8	16.00	15.25	15.08	0.006	0.005	0.004	
600	05:40:14.17	-69:45:09.8	19.28	18.17	17.72	0.021	0.014	0.011	
601	05:40:14.24	-69:43:50.2	17.17	16.26	15.95	0.010	0.014	0.020	
602	05:40:14.27	-69:44:36.6	18.40	17.30	16.86	0.011	0.010	0.012	
603	05:40:14.38	-69:43:44.0	17.91	17.25	17.14	0.009	0.015	0.025	
604	05:40:14.45	-69:44:25.5	19.37	18.82	18.67	0.022	0.022	0.027	
606	05:40:14.52	-69:43:42.1	19.44	19.01	18.84	0.024	0.036	0.047	
607	05:40:14.51	-69:45:35.5	15.89	14.95	14.75	0.010	0.006	0.017	
608	05:40:14.53	-69:44:45.7	19.87	18.73	18.38	0.032	0.023	0.022	
609	05:40:14.59	-69:44:50.4	19.08	17.82	17.29	0.019	0.012	0.010	
610	05:40:14.62	-69:45:24.6	16.77	15.90	15.71	0.009	0.006	0.009	
611	05:40:14.69	-69:44:52.5	19.38	18.90	18.72	0.029	0.026	0.038	
612	05:40:14.78	-69:44:05.7	19.01	17.92	17.47	0.020	0.020	0.021	
613	05:40:14.82	-69:44:31.5	19.44	18.68	18.25	0.029	0.019	0.018	
614	05:40:14.98	-69:45:35.8	19.50	18.93	18.91	0.030	0.034	0.036	
616	05:40:15.00	-69:44:01.5	18.00	17.63	17.58	0.010	0.018	0.031	
617	05:40:15.00	-69:44:17.2	17.52	16.91	16.79	0.009	0.014	0.016	
618	05:40:15.02	-69:44:08.5	17.73	17.07	16.96	0.009	0.013	0.019	
619	05:40:15.22	-69:44:33.2	19.61	18.66	18.30	0.028	0.020	0.022	
620	05:40:15.28	-69:44:10.7	16.46	15.75	15.61	0.005	0.010	0.016	
621	05:40:15.36	-69:45:42.7	18.13	17.72	17.71	0.029	0.027	0.078	
623	05:40:15.58	-69:44:04.8	19.25	18.03	17.56	0.023	0.020	0.021	
624	05:40:15.58	-69:45:38.6	18.21	17.51	17.34	0.013	0.011	0.018	
625	05:40:15.64	-69:44:52.8	19.95	19.24	19.17	0.037	0.032	0.039	
626	05:40:15.69	-69:44:10.4	19.61	18.52	18.16	0.022	0.020	0.024	
627	05:40:15.77	-69:45:14.3	18.06	17.88	17.90	0.011	0.013	0.014	
628	05:40:15.86	-69:44:06.1	19.32	18.64	18.31	0.020	0.023	0.023	
629	05:40:15.94	-69:44:13.3	18.29	17.25	16.82	0.013	0.016	0.020	
630	05:40:15.95	-69:43:50.5	15.65	14.46	14.16	0.007	0.013	0.021	
631	05:40:16.00	-69:43:44.5	19.55	18.53	18.33	0.021	0.027	0.035	
632	05:40:16.13	-69:44:21.2	19.18	18.09	17.67	0.018	0.017	0.025	
633	05:40:16.14	-69:43:34.0	18.63	18.10	17.92	0.016	0.028	0.040	
634	05:40:16.37	-69:44:13.5	16.18	15.02	14.68	0.008	0.011	0.017	
635	05:40:16.38	-69:45:10.8	19.62	18.92	18.86	0.028	0.027	0.032	